Ecological Monographs, 84(2), 2014, pp. 329–353

Biophysical forcings of land-use changes from potential forestry activities in North America

Kaiguang Zhao[1,2,4] and Robert B. Jackson[1,3]

[1]*Division of Earth and Ocean Sciences and Center on Global Change, Nicholas School of the Environment, Duke University, Durham, North Carolina 27708 USA*
[2]*School of Environment and Natural Resources, Ohio Agricultural Research and Development Center, The Ohio State University, Wooster, Ohio 44691 USA*
[3]*School of Earth Sciences, Woods Institute for the Environment, and Precourt Institute for Energy, Stanford University, Stanford, California 94305 USA*

Abstract. Land-use changes through forestry and other activities alter not just carbon storage, but biophysical properties, including albedo, surface roughness, and canopy conductance, all of which affect temperature. This study assessed the biophysical forcings and climatic impact of vegetation replacement across North America by comparing satellite-derived albedo, land surface temperature (LST), and evapotranspiration (ET) between adjacent vegetation types. We calculated radiative forcings (RF) for potential local conversions from croplands (CRO) or grasslands (GRA) to evergreen needleleaf (ENF) or deciduous broadleaf (DBF) forests. Forests generally had lower albedo than adjacent grasslands or croplands, particularly in locations with snow. They also had warmer nighttime LST, cooler daily and daytime LST in warm seasons, and smaller daily LST ranges. Darker forest surfaces induced positive RFs, dampening the cooling effect of carbon sequestration. The mean (±SD) albedo-induced RFs for each land conversion were equivalent to carbon emissions of 2.2 ± 0.7 kg C/m^2 (GRA–ENF), 2.0 ± 0.6 kg C/m^2 (CRO–ENF), 0.90 ± 0.50 kg C/m^2 (CRO–DBF), and 0.73 ± 0.22 kg C/m^2 (GRA–DBF), suggesting that, given the same carbon sequestration potential, a larger net cooling (integrated globally) is expected for planting DBF than ENF. Both changes in LST and ET induce longwave RFs that sometimes had values comparable to or even larger than albedo-induced shortwave RFs. Sensible heat flux, on average, increased when replacing CRO with ENF, but decreased for conversions to DBF, suggesting that DBF tends to cool near-surface air locally while ENF tends to warm it. This local temperature effect showed some seasonal variation and spatial dependence, but did not differ strongly by latitude. Overall, our results show that a carbon-centric accounting is, in many cases, insufficient for climate mitigation policies. Where afforestation or reforestation occurs, however, deciduous broadleaf trees are likely to produce stronger cooling benefits than evergreen needleleaf trees provide.

Key words: albedo effect; biophysical forcing; carbon accounting; carbon sequestration; climate regulation; ecosystem services; forestry; land-use change; radiative forcing.

Introduction

Accompanying the need to combat global warming is an increasing interest in how ecosystems regulate climate (e.g., Heimann and Reichstein 2008). Along with traditional goods and services, such as biodiversity conservation and watershed protection, the climatic benefits of ecosystems are generally assessed from a carbon-centric perspective (McAlpine et al. 2010). Alterations to ecosystems can indeed change carbon sinks or sources that dampen or accelerate global warming. Since 1850, for instance, land-use change has released ~150 billion metric tons of carbon, accounting for 35% of anthropogenic CO_2 emissions (Houghton 2003). Safeguarding and enlarging terrestrial carbon pools are thus key strategies to mitigate climate change, typically through forestry practices such as reforestation, afforestation, avoided deforestation, and forest management (e.g., Jackson and Baker 2010, McKinley et al. 2011).

Land alterations by forestry and other activities modify not only carbon stocks, but also energy partitioning, water cycling, and atmospheric composition (Fig. 1). These changes occur through altered biophysical characteristics, including albedo, surface roughness, sensible and latent heat fluxes, canopy conductance, soil moisture, surface temperature, emissivity, leaf area, and rooting depth (Kueppers et al. 2007, Anderson et al. 2011, Jayawickreme et al. 2011). For instance, forested surfaces often have lower albedo and more uneven canopies compared to other vegetation, absorbing more sunlight and facilitating the mixing

Manuscript received 2 October 2012; revised 6 August 2013; accepted 11 September 2013; final version received 19 October 2013. Corresponding Editor: A. O. Finley.
[4] E-mail: zhao.1423@osu.edu

of air (Betts 2000). Locally, these climate forcings affect temperature more than the CO_2 reduction does. At regional and global scales, biophysical forcings can either amplify or diminish the cooling benefit of carbon uptake. Because of such interactions, researchers have recently recommended that climate policies for crediting forestry projects should go beyond a carbon-centric accounting to include biophysical effects (Jackson et al. 2008, Montenegro et al. 2009, McAlpine et al. 2010).

Although considerations of both biophysical and biogeochemical mechanisms are undoubtedly important in formulating policies to optimize climate benefits of forestry or land management activities, the science for such integration is still evolving (e.g., West et al. 2011). One unresolved issue is how best to capture the spectrum of climate forcings for biophysical and biogeochemical processes that tend to occur at vastly different spatial and temporal scales (Bonan 2008). For instance, the climate effects of carbon sequestration are global and long lasting and are quantified primarily in terms of radiative influences on global mean temperatures. In contrast, biophysical impacts are dominantly local or regional; they occur with altered lands and diminish if the lands revert. Biophysical changes also exert both radiative and non-radiative influences, modifying air temperatures and hydrologic cycles. These disparities in mechanisms raise issues as to how to combine biophysical and biogeochemical regulations into policy measures for climate change mitigation.

Comparisons of carbon sequestration and biophysics for climate regulation by ecosystems are typically assessed in terms of radiative forcing (RF), defined as the perturbation to the radiation balance of the climate system (Betts 2000, Rotenberg and Yakir 2010). With tree planting, reduced albedo and carbon uptake typically cause a positive shortwave (warming) and a negative longwave (cooling) RF, respectively. The opposite is often true when clearing forests for other land uses. Agricultural land use during the past 300 years is estimated to have led to a global RF of -0.15 W/m^2 and a cooling of -0.09°C due to biophysical effects (Matthews et al. 2003). Additionally, climatic consequences of natural disturbances to forests, such as fire, insect infestation, windfall, and drought, have been examined with RF or its equivalent carbon metrics, incorporating the effects of both carbon release and albedo change (O'Halloran et al. 2011).

Vegetation replacement also alters the exchange of energy and matter between ecosystems and the atmosphere, particularly through the re-partitioning of sensible and latent heat (Juang et al. 2007). These non-radiative forcings modify the boundary layer and influence local climate (West et al. 2011). Increased sensible heat flux warms the near-surface air and the mixed layer directly. Increased evapotranspiration (ET) of trees not only moistens the air, but can also offset the extra solar absorption incurred by lower albedo (Nosetto et al. 2011), thus tending to cool the surface locally and sometimes the near-surface air. This evaporative cooling varies with season and place, being most pronounced in tropical forests (Anderson et al. 2011). Moreover, alterations in ET mediate land-air interactions through potential changes in lapse rate, longwave RF, and cloudiness.

Observations and earth-system models are both powerful tools for examining the climatic footprint of land-use change (Bonan 2008). For instance, climate simulations indicated a global cooling effect from replacing short vegetation with forest, attributable mainly to the enhanced ET that fostered low-level cloudiness and attenuated sunlight (Ban-Weiss et al. 2011). Paired model simulations have also suggested that deforestation should be avoided in the tropics and reforestation discouraged at high latitudes to harness climatic benefits of trees, although the latter result is controversial (Randerson et al. 2006, Bala et al. 2007). Meanwhile, differences in climate model structure and parameterization sometimes generate conflicting results (Jackson et al. 2005, Diffenbaugh 2009). In particular, uncertainties exist as to whether the biophysical effects of reforestation in temperate zones will strengthen or weaken the cooling from carbon sequestration (Betts 2000, Jackson et al. 2008, Montenegro et al. 2009).

Despite growing recognition of the biophysical regulation of climate by ecosystems, quantifying their effects is challenging for academic researchers, let alone for resource managers and policy makers (McAlpine et al. 2010, West et al. 2011). Existing efforts to quantify biophysical regulations have typically considered albedo but neglected other important biophysical forcings. For instance, altered ET and land surface temperature (LST) induce longwave RFs that can sometimes be comparable to the albedo-induced shortwave RF (Swann et al. 2010). Improved assessments are needed for biophysical forcings of land-use changes and their policy implications.

We combined remotely sensed observations and climate model outputs to examine the biophysical forcings and climatic impacts of potential land-use/land-cover changes across North America. We emphasized transitions from non-forest to forest vegetation relevant to climate mitigation policies, specifically cropland (CRO) and grassland (GRA) conversions to evergreen needleleaf forest (ENF) and deciduous broadleaf forest (DBF). We examined surface variables important for temperature and energy balance, including albedo, LST, and ET (Table 1). We evaluated the magnitudes and directions of differences in these biophysical variables between adjacent sites of contrasting vegetation across North America between 20°–60° N, using paired comparisons to assess the changes in surface biophysics associated with land conversions. Observed differences were then used to (1) calculate shortwave and longwave RFs or equivalent carbon emissions, (2) infer the redistribution of surface energy for conversions from GRA or CRO to ENL or DBF,

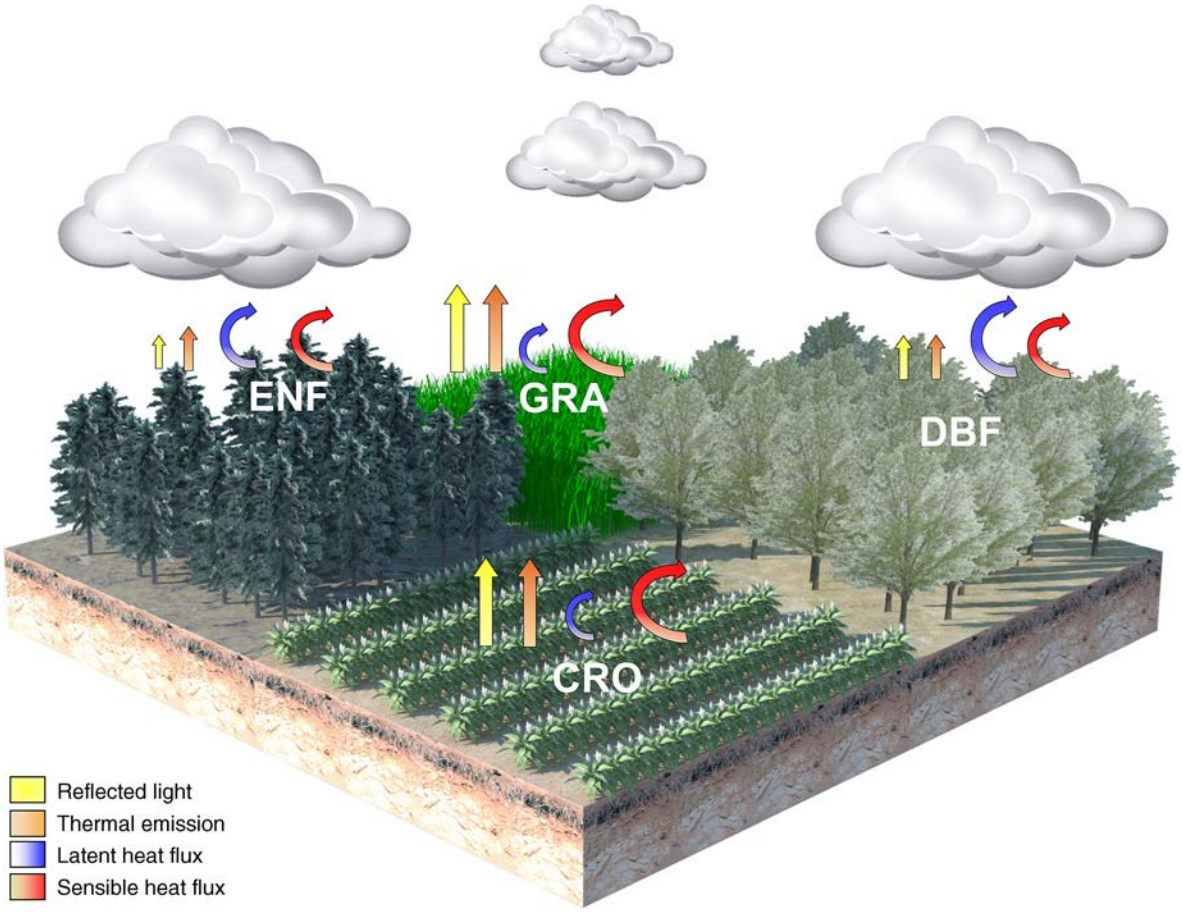

FIG. 1. Besides carbon, biophysics matters in assessing climate benefits of forestry projects: Forests and non-forest vegetation have contrasting biophysical properties, resulting in differing land–air interactions. Compared to non-forest lands, forests typically (1) have lower albedo and absorb more solar energy; (2) often have higher surface roughness, facilitating the exchange of water and heat between surfaces and the air; (3) are often cooler, emitting less thermal radiation; and (4) have higher leaf areas and deeper roots, likely increasing evapotranspiration. Larger latent heat fluxes and smaller sensible heat fluxes over forests can decrease the lifting condensation level (cloud base height), thus lowering cloud height and increasing the chance for cloud formation. The relative magnitudes of surface energy fluxes for the four vegetation types studied here (grasslands [GRA], deciduous forests [DBF], croplands [CRO], and evergreen forests [ENF], as depicted clockwise from the top in the graph) are indicated by the sizes of arrows. These biophysical differences highlight that reforestation and afforestation impact climate via biophysical pathways in addition to carbon sequestration.

and (3) assess potential impacts on near-surface temperature. A primary goal of our work is to foster a more complete accounting of climate regulation for ecosystem and land-use management and policy mitigation.

METHODS

Data

This study focused on the vegetated lands of North America between 20°–60° N including the conterminous USA (Appendix: Fig. A1). A range of surface and atmospheric variables derived from remote-sensing observations was compiled from three geoportals: the Moderate-Resolution Imaging Spectroradiometer (MODIS; data *available online*)[5] land surface products, the Clouds and the Earth's Radiant Energy System (CERES; data *available online*)[6] data archive, and the Advanced Microwave Scanning Radiometer-Earth Observing System (AMSE-E; data *available online*).[7] The MODIS data we used comprised yearly land cover (MOD12Q1; Friedl et al. 2002), eight-day 500-m bidirectional reflectance distribution function (BRDF)/Albedo (MCD43A1 and A2 Collection 5; Schaaf et al. 2002), eight-day 1-km daytime and nighttime LSTs (MOD11A2 Collection 5; Wan et al. 2004), and eight-day 1-km ET (MOD16A2; Mu et al. 2011). The MODIS land-cover data included both 500-m Collection-5 maps for years 2000–2008 and a 1-km Collection-4 map for the year 2001 (Friedl et al. 2002), with the latter being used as a baseline vegetation map for

[5] https://lpdaac.usgs.gov/data_access

[6] https://eosweb.larc.nasa.gov

[7] http://nsidc.org/data/ae_dysno

TABLE 1. Major concepts and terms pertinent to the quantification of biophysical forcings of land-use change from forestry activities, with common units supplied whenever applicable.

Concepts and terms	Common units	Explanation
Climate regulation		Ecosystems offer regulating services by influencing climate via both biogeochemical and biophysical pathways.
Climate forcing	W/m^2	An energy imbalance imposed on the climate system either naturally or by human activities, such as C emissions arising from altered ecosystem structure.
Radiative forcing	W/m^2	The change in radiative energy flux resulting from climate forcing agents such as a CO_2 increase or albedo change. Positive radiative forcings, either longwave or shortwave, increase global mean temperature.
Climate sensitivity	$K/[W/m^2]$	A measure of how responsive the climate system is to the radiative forcing of a forcing agent. It is often quantified as the increase in global mean air temperature given a unit of radiative forcing
Climate efficacy	unitless	The global temperature response per unit radiative forcing of an agent relative to that of CO_2. It is defined as the ratio of climate sensitivity between a forcing agent and CO_2 change.
Non-radiative forcing	W/m^2	An energy imbalance that does not directly involve radiation, such as the increase in evapotranspiration due to irrigation.
Biophysical forcing	W/m^2	The imbalance of energy fluxes resulting directly or indirectly from changes in biophysics, including albedo, emissivity, sensible and latent heat, and surface roughness. These biophysical changes can be caused by both natural and anthropogenic processes such as land conversion, ecosystem disturbances, and ecosystem management.
Albedo	unitless	Reflectivity of sunlight by land surfaces, as contributed from both soils and vegetation. Conversions of croplands or grasslands to forests often reduce surface albedo and induce positive shortwave radiative forcings, diminishing the cooling benefit of forest carbon sequestration.
Emissivity	unitless	The relative ability of land surfaces to emit thermal radiation. Forests often have slightly higher emissivity than do croplands or grasslands. The biophysical forcing of altered emissivity from land-use change is typically much smaller than that of altered albedo.
Sensible heat flux	W/m^2	The flux of heat between land and the air via conduction and convection. Sensible heat directly warms the air. Altered sensible heat flux due to vegetation shift is a direct warming or cooling effect on local climate.
Latent heat flux	W/m^2	The flux of heat between land and the air via evapotranspiration or condensation. Latent heat doesn't directly warm the air. Altered latent heat flux due to vegetation shift is a nonlocal biophysical forcing, which modifies surface energy balance, the hydrological cycle, atmospheric water vapor, and cloud formation.
Land surface temperature	K or °C	The temperature of the composites of vegetation and soils over vegetated surfaces, which can be defined either radiometrically, thermodynamically, or aerodynamically. Changes in vegetation structure affect surface energy partitioning and thus strongly affect land surface temperature.
Near-surface air temperature	K or °C	The temperature of the air two meters above a vegetation-specific displacement height for a vegetated surface. This is the temperature metric used here to directly evaluate the temperature effect of land-use change.
C sequestration potential	$kg\ C/m^2$ or $kg\ C \cdot m^{-2} \cdot yr^{-1}$	The amount of carbon potentially drawn from the air for a given forestry project due to biological carbon sequestration. Its exact value is difficult to estimate and in this study is considered simply as the difference in steady-state total carbon stock between the forest and the replaced vegetation.
Carbon-emission equivalent	$kg\ C/m^2$ or $kg\ C \cdot m^{-2} \cdot yr^{-1}$	The amount of hypothetical carbon emission that can cause the same change in global mean temperature as the temperature change due to biophysical forcings. It helps to quantify the temperature effects of biophysical forcings in terms of carbon. Negative carbon emission equivalent represents a carbon sink, suggesting a global cooling effect from the biophysical forcings.
Net carbon drawdown	$kg\ C/m^2$ or $kg\ C \cdot m^{-2} \cdot yr^{-1}$	The difference between C sequestration potential and C-emission equivalent as a C metric to assess the combined effect of biological carbon sequestration and biophysical forcings on temperature for forestry projects. It can serve as an index to quantify the climate regulation value of ecosystems.
Greenhouse gas value	$kg\ C/m^2$ or $kg\ C \cdot m^{-2} \cdot yr^{-1}$	An integrated quantification of climate regulation services in terms of C equivalents. The integration typically encompasses diverse factors, including biophysical forcings, fluxes of greenhouse gases, the carbon footprints of operations and energy costs, and carbon leakage from disturbances. Conversions of individual factors to carbon emissions often occur through the concept of global warming potential for non-CO_2 greenhouse gases, as used in life-cycle analysis and other comparative frameworks.

generating the MODIS ET time series products (Mu et al. 2011). The CERES data included monthly averaged products of top of atmosphere (TOA)/surface longwave and shortwave fluxes and monthly gridded cloud products, with a spatial resolution of $1^\circ \times 1^\circ$ (Wielicki et al. 1998). The advanced microwave scanning radiometer-EOS (AMSR-E) data included the five-day Level 3 global snow water equivalent (SWE) at 25-km resolution (Kelly et al. 2003).

For each product, we analyzed all available data for the most recent version as of December 2011. All products except MODIS ET were retrieved directly from satellite radiometric signals using dedicated algorithms; the MODIS ET product was derived using an empirical Penman-Monteith model by Mu et al. (2007) from meteorological and remote-sensing observed inputs such as air temperature and leaf area index. The theoretical basis, retrieval algorithms, and data validation for each product are available from the citations in the preceding paragraph. In particular, MODIS albedo and LST products have proven useful for characterizing biophysical variables of contrasting land surfaces at pixel scales (e.g., Montenegro et al. 2009). We also used two ancillary datasets: the 90-m digital evaluation model (DEM) from the Shuttle Radar Topography Mission (SRTM; data *available online*)[8] and the ratio of diffuse/direct downward surface shortwave fluxes calculated from a one-year model simulation using the coupled Weather Research Forecast-Community land model (WRF-CLM; Lu and Kueppers 2012).

Comparisons of surface biophysics between contrasting vegetation

MODIS products were used primarily to evaluate differences in surface albedo, LST, and ET between contrasting vegetation types (Table 1). Our evaluations emphasized paired adjacent sites (i.e., pixels) for two contrasting vegetation types. These adjacent sites were most likely to be found in ecotones and disturbed lands where the potential of future land-cover changes due to either natural processes or human activities is high. By using adjacent sites, we attempted to isolate vegetation controls on surface biophysics to the greatest extent possible and to minimize the influences of confounding factors such as topography, solar angle, and rainfall. Such comparisons are particularly relevant for land-use/land-cover change because forestry conversions occur mostly at small scales. Differences between adjacent pixels/sites should also mimic future changes in surface biophysical characteristics with vegetation replacement.

Because we were interested mainly in comparing typical differences in biophysical variables for vegetation types, MODIS products such as albedo, ET, and LST were averaged across years from 2001 to 2011 for each of the 46 eight-day observation periods to smooth out interannual variability. In this averaging, the 11 MODIS quality-control flags associated with years 2001–2011 for each pixel and eight-day observation period were checked to select the years that had the best data quality; if the number of years with the best quality was less than five out of 11, we gradually incorporated the years with the next best quality; however, these years were assigned a weighting factor only half that of the higher quality years. This weighted-averaging procedure helped to reduce random errors and any quality-control issues in the MODIS products.

To determine the spatial distributions of vegetation, we derived a land-cover map at 500-m resolution by synthesizing the nine yearly 500-m MODIS land-cover layers for 2001–2008. A pixel was assigned a particular vegetation class only if the pixel was classified as this class with at least a probability of 0.50 for more than five out of nine years; otherwise, the pixel was discarded from our analysis. This filtering helped to suppress the confounding effects of classification errors and potential land-cover changes that occurred between 2001 and 2008. Additionally, the resultant 500-m base map was aggregated to 1-km resolution, with a 1-km pixel labeled as a vegetation class only if its four 500-m component pixels all belonged to the same class; otherwise, the pixel was discarded from our analysis. The 500-m and 1-km land-cover maps each contain a total of 17 land-cover types, but we considered only four vegetation types: CRO, GRA, ENF, and DBF. The two synthesized maps helped to derive vegetation-specific albedo and LST at 500-m and 1-km resolutions, respectively. However, vegetation-specific ET was derived based on the third map, the 2001 1-km MODIS Collection-4 land cover, because it is the reference map for generating MODIS ET (Mu et al. 2011).

The adjacent sites chosen to compare biophysical variables between contrasting vegetation types were determined based on the three land-cover maps using a customized local searching-window procedure. To suppress topographic influences, we considered only the sites with slopes of $<15^\circ$. Using comparisons of albedo between DBF and CRO to illustrate this procedure, for each DBF pixel, all the CRO pixels within a 15-km radius of it were identified and a DEM filter was applied to select only those CRO pixels that had elevation differences <10 m from the reference DBF pixel. The average albedo over all the final CRO pixels was then computed and compared against that for the reference DBF pixel. This local-scale comparison could also be performed using CRO pixels as the reference; our results showed that both potential choices of reference class gave essentially identical results. Additionally, this circular window of 30 km in diameter was moved across the study area to identify all the possible pairs of adjacent sites of contrasting vegetation.

Of the MODIS surface biophysical variables studied here, albedo depends not only on vegetation and soil properties, but also on solar angle and atmospheric conditions. To isolate the dependence of albedo on surface characteristics, we considered MODIS broad-

[8] http:srtm.usgs.gov/index.php

band white-sky albedo in our comparisons of paired sites. White-sky albedo is also called diffuse albedo, representing bi-hemispherical reflectance under isotropic skylight illumination; therefore, it is independent of sky conditions (Schaaf et al. 2002). ET is often constrained by water availability. Currently, the MODIS ET algorithm did not explicitly differentiate between irrigated and nonirrigated lands (Mu et al. 2011). However, the algorithm has synthesized information from some input variables responsive to soil water content; therefore, it indirectly captured the effect of irrigation such that irrigated lands in the MODIS ET often have high ET. To examine the spatial patterns of differences in albedo or ET, we applied the *k*-means algorithm to group the paired sites associated with each pair of vegetation types into three spatial clusters based on the similarity of seasonal variations in albedo or ET. More importantly, differences in biophysical variables between contrasting vegetation at the paired sites were used to evaluate biophysical forcings for potential vegetation shifts. These included shortwave and longwave radiative forcings and changes in surface sensible and latent heat fluxes, as detailed in the next four subsections.

Shortwave radiative forcing (SF) induced by albedo change

Altered surface albedo from land-use change induces shortwave RF, often evaluated at three levels: surface, atmosphere, and top of atmosphere (TOA). Specifically, RF at the surface (SF_{sfc}) affects the surface energy balance and partitioning. RF at the TOA (SF_{toa}) is the quantity related to the change in global mean temperature through climate sensitivity parameters. Atmospheric RF (SF_{atm}) is the difference between TOA and surface RFs (i.e., $SF_{atm} = SF_{toa} - SF_{sfc}$); it represents the radiative imbalance of the atmospheric column and provides information on expected changes in precipitation and vertical mixing. Considerations of the vertical structure of RF have been recently requested for future climate assessments by the U.S. National Research Council (2005), although TOA RF still remains the most commonly used metric for quantifying and ranking the climatic impacts of different forcing agents. Calculations of TOA RF (SF_{toa}) require translating surface albedo (α_{sfc}), as measured by MODIS, to planetary albedo at the TOA (α_{toa}), generally with α_{sfc} contributing to only a small fraction of α_{toa}. This translation requires vertical profiles of atmospheric optical properties as determined by atmospheric compositions such as aerosol and cloud cover.

The single-layer radiative transfer model of Liou (2002) offers a simple yet effective scheme relating surface α_{sfc} to TOA albedo, α_{toa}. This model uses two column-integrated optical parameters, namely, single-pass atmospheric reflectance R and transmittance T. We extended this model to further discriminate clear and cloudy skies within a grid as follows:

$$\begin{aligned}\alpha_{toa}(\alpha_{sfc}) &= \frac{F^{\uparrow}_{toa}}{S} \\ &= cR_{cld} + (1-c)R_{clr} + c\alpha_{sfc}\frac{T^2_{cld}}{1-\alpha_{sfc}R_{cld}} \\ &\quad + (1-c)\alpha_{sfc}\frac{T^2_{clr}}{1-\alpha_{sfc}R_{clr}} \end{aligned} \quad (1)$$

where S and $F^{\uparrow}_{toa}$ are the incident and reflected solar fluxes at the TOA, respectively; c is the fraction of cloud cover; R_{cld} and T_{cld} are the single-pass atmospheric reflectance and transmittance for the cloudy sky, respectively; and R_{clr} and T_{clr} are for the clear sky. The sum of the first two terms $cR_{cld} + (1 - c)R_{clr}$ is treated as the atmospheric contribution to TOA albedo α_{toa}, whereas the sum of the last two terms is the surface contribution to α_{toa}. Accordingly, the relative fraction of surface albedo contributed to TOA albedo is calculated as

$$\left[c\alpha_{sfc}\frac{T^2_{cld}}{1-\alpha_{sfc}R_{cld}} + (1-c)\alpha_{sfc}\frac{T^2_{clr}}{1-\alpha_{sfc}R_{clr}}\right] \Big/ \alpha_{sfc}.$$

Further, downward and upward shortwave fluxes (sunlight) at the surface are given by

$$F^{\downarrow}_{sfc}(\alpha_{sfc}) = S \times \left[c\frac{T_{cld}}{1-\alpha_{sfc}R_{cld}} + (1-c)\frac{T_{clr}}{1-\alpha_{sfc}R_{clr}}\right]$$

$$F^{\uparrow}_{sfc}(\alpha_{sfc}) = \alpha_{sfc}F^{\downarrow}_{sfc}(\alpha_{sfc}). \quad (2)$$

The dependences of TOA and surface fluxes on albedo α_{sfc} have been made explicit on the left-hand side of Eqs. 1 and 2.

Following a method similar to Donohoe and Battisti (2011), we estimated the atmospheric reflectance R and transmittance T of Eqs. 1 and 2 for both the clear and cloudy sky portions monthly for each $1^\circ \times 1^\circ$ grid, using the CERES daytime cloud cover data and the CERES cloudy-sky and clear-sky TOA/surface shortwave fluxes. Our estimated atmospheric reflectance R and transmittance T characterize the actual atmospheric optical properties and allow us to compute surface, TOA, and atmospheric shortwave RFs as follows:

$$SF_{toa} = -S \times \left[\alpha_{toa}(\alpha_{sfc,2}) - \alpha_{toa}(\alpha_{sfc,1})\right]$$

$$SF_{sfc} = F^{\downarrow}_{sfc}(\alpha_{sfc,2}) \times (1-\alpha_{sfc,2}) - F^{\downarrow}_{sfc}(\alpha_{sfc,1}) \times (1-\alpha_{sfc,1})$$

$$SF_{atm} = SF_{toa} - SF_{sfc}. \quad (3)$$

Here, the RFs are driven by a change in surface albedo from $\alpha_{sfc,1}$ to $\alpha_{sfc,2}$ while assuming that the atmospheric optical properties, including c, R, and T, remain unaffected. A positive shortwave RF in Eq. 3 indicates that the system absorbs extra solar radiation after land conversion. Eqs. 1–3 are applicable for computing instantaneous or short-time RFs that can then be integrated to estimate long-term RFs such as annual RFs.

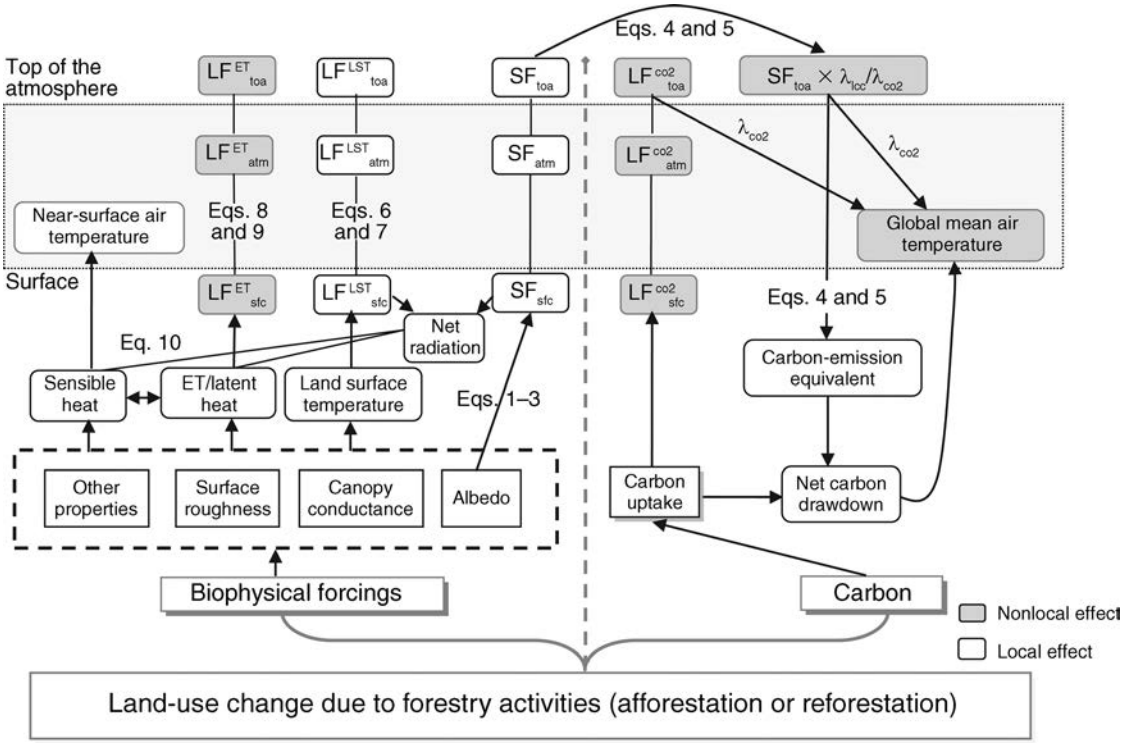

FIG. 2. Schematic of the major biophysical forcings we examined: Land-use change by forestry alters the surface biophysics to induce both radiative and non-radiative forcings (left) that modify the cooling effect of forest carbon uptake (right). Radiative forcings, either shortwave (SF) or longwave (LF), perturb the radiation balance at the surface (sfc) and the top of the atmosphere (toa), or within the atmosphere column (atm). Non-radiative biophysical forcings exert strong controls on the redistribution of surface energy. In particular, enhanced evapotranspiration (ET) from forests lowers land surface temperature (LST) while a reduced input of sensible heat to the air tends to cool the near-surface air locally. The relative magnitudes of the competing effects of reduced albedo and carbon storage associated with reforestation and afforestation is often gauged by a metric called net carbon drawdown. In the schematic, gray-filled boxes denote components whose influences are not locally confined to the converted land. The equations we used are also labeled; λ_{lcc} and λ_{CO_2} denote climate sensitivities for land use and CO_2 changes, respectively. As an observation-based study, our analyses do not capture all the feedbacks and interactions between land and the atmosphere.

Using Eqs. 1–3, we calculated monthly RFs for four scenarios of non-forest to forest conversions (GRA or CRO to ENF or DBF) at a $1° \times 1°$ resolution, compatible with the spatial and temporal resolutions of R and T derived from the CERES data. In the calculation, we considered actual surface albedo for α_{sfc}, which was estimated as the average of MODIS black-sky (direct) and white-sky (diffuse) albedos weighted by direct and diffuse downward fluxes from the regional climate simulation of WRF-CLM. Also importantly, albedos of adjacent sites as obtained from local comparisons of paired vegetation types were used in Eq. 3 for $\alpha_{sfc,1}$ and $\alpha_{sfc,2}$ to mimic realistic local vegetation shifts. The albedo values of all the paired sites within each $1° \times 1°$ grid were averaged, and the resulting mean albedos were then applied to Eq. 3 for estimating the grid-level RF. Only those grids containing at least three pairs of adjacent sites were considered.

Carbon emission equivalent to albedo change

Albedo-induced shortwave RF at the TOA (SF_{toa}; in W/m^2) is often converted to carbon emission equivalent (δC_{alb}; in kg/m^2), a C density that can be compared against the C sequestration potential δC_{seq} of land management to contrast biogeochemical and biophysical effects (Fig. 2). To date, the standard conversion method has generally overlooked the fact that the RFs from altered albedo and CO_2 manifest different vertical structures, so that the same amount of RFs from these two forcing agents leads to different changes in global mean temperature (Betts 2000). Typically, these differing responses are characterized by climate sensitivity (λ), defined as the change in global mean temperature per unit RF for a forcing agent and taken here as $\lambda_{alb} = 0.52$ $K/(W/m^2)$ for albedo and $\lambda_{co2} = 1.0$ $K/(W/m^2)$ for CO_2 (Davin et al. 2007). Accounting for this disparity may alter the conclusions of some earlier studies that assumed the same climate sensitivity for the two types of RFs in evaluating temperature benefits of reforestation.

We revised the standard method of converting RF SF_{toa} to carbon-emission equivalent δC_{alb} by differentiating the two climate sensitivity parameters λ_{alb} and λ_{co2}. For a RF of SF_{toa} resulting from albedo change

over a local area s_{lcc} (m^2), the total radiative perturbation is $SF_{toa} \cdot s_{lcc}$, which becomes $SF_{toa} \cdot (s_{lcc}/S_E)$ if spread evenly across the globe with $S_E = 5.1 \times 10^{14}$ m^2 being the total surface area of the Earth. Further, this global shortwave RF is multiplied by the ratio of climate sensitivity $\lambda_{alb}/\lambda_{co2}$ to obtain an effective CO_2-induced longwave RF $SF_{toa} \cdot (s_{lcc}/S_E) \cdot \lambda_{alb}/\lambda_{co2}$. The ratio $\lambda_{alb}/\lambda_{co2}$ is often termed the climate efficacy (Hansen et al. 2005) and is applied here to ensure that the two types of RFs yield the same amount of global temperature response according to their respective climate sensitivities. Then, the effective global longwave RF, $SF_{toa} \cdot (s_{lcc}/S_E) \cdot \lambda_{alb}/\lambda_{co2}$, is converted to a change in atmospheric CO_2 concentration δC_{co2} (parts per million per volume [ppmv]) via the efficiency parameter of 5.35 W/m^2 as follows:

$$\delta C_{co2} = \left(\exp^{SF_{toa} \times \frac{\lambda_{alb}}{\lambda_{co2}} \times \frac{s_{lcc}}{S_E} \times \frac{1}{5.35}} - 1 \right) \times C_{co2} \quad (4)$$

where $C_{co2} = 391$ ppmv is the reference CO_2 concentration. Finally, the CO_2 change δC_{co2} is translated to the land C emission δC_{alb} (kg/ m^2) over the area s_{lcc} as follows:

$$\delta C_{alb} = \frac{\kappa \times \delta C_{co2}}{0.50} \frac{1}{s_{lcc}} \approx C_{co2} \times \frac{\kappa \times SF_{toa}}{0.50 \times 5.35 \times S_E}$$

$$= 0.611 \times \frac{\lambda_{alb}}{\lambda_{co2}} \times SF_{toa} \quad (5)$$

where the constant of 0.50 in the denominator is the airborne fraction, representing the portion of C emission that remains in the air after being absorbed by the ocean and other terrestrial sinks (Betts 2000, Montenegro et al. 2009), and κ (2.13×10^{12} kg/ppmv) is the coefficient converting C from ppmv to kg. The term δC_{alb} refers to the emission of carbon and can be converted to a CO_2 equivalent by multiplying by 3.67.

The C emission equivalent δC_{alb} converted from SF_{toa} can be used to adjust the actual C sequestration potential of forests δC_{seq}, which results in a net carbon drawdown metric (i.e., $\delta C_{seq-alb} = \delta C_{seq} - \delta C_{alb}$) for quantifying the temperature benefit of forestry projects. The value of δC_{alb} is typically positive for conversions to forests because of the reduced albedo and increased shortwave absorption in consequence; it represents the minimum C uptake that the trees need to sequester compared to the replaced vegetation for offsetting the warming of reduced albedo. Therefore, positive net carbon drawdown (i.e., $\delta C_{seq-alb} > 0$) indicates a global cooling in terms of the integrated effects of albedo reduction and CO_2 uptake. Calculating net carbon drawdown $\delta C_{seq-alb}$ requires the actual C sequestration potential δC_{seq}, a quantity often estimated as the difference in steady-state C stocks before and after land conversion. However, to our knowledge no reliable data sets are available for spatially explicit mapping of C stocks of different vegetated lands at a scale commensurate with the satellite data we used, especially for belowground carbon. Moreover, the definitions and calculations of carbon sequestration, δC_{seq}, for forestry projects varied considerably among prior studies, particularly concerning how the studies treated land-use history and forest management practices. Therefore, we did not estimate exact values of δC_{seq} or $\delta C_{seq-alb}$, but just inferred the potential signs of net carbon drawdown $\delta C_{seq-alb}$ by referring to previous estimates of approximate C sequestration potential, δC_{seq}, of forestry projects (Betts 2000, Claussen et al. 2001, Gibbard et al. 2005, Montenegro et al. 2009).

Longwave radiative forcing induced by changes in surface temperature/emissivity and ET

Altered surface biophysical properties modify the longwave radiative regime through at least two mechanisms, one pertinent to LST and emissivity and another to ET (Fig. 2). Specifically, surface longwave RF from the altered LST and emissivity is defined as the change in net downward longwave radiation at the surface and is calculated by

$$LF_{sfc}^{LST} = (\varepsilon_1 \sigma_1 T_1^4 - \varepsilon_2 \sigma_2 T_2^4) + L^{\downarrow}(\varepsilon_2 - \varepsilon_1) \quad (6)$$

where T_1 and T_2 denote LSTs before and after land conversion, with the corresponding emissivity being ε_1 and ε_2; $L^{\downarrow}$ is the downward sky longwave flux and is assumed to be unchanged; and σ (5.67×10^{-8} $W \cdot m^2 \cdot K^{-4}$) is the Stefan-Boltzmann constant. Of the two surface terms in Eq. 6, the first, attributable mainly to the temperature change, dominates, whereas the second, attributable to the emissivity change, is small and often negligible. A positive value of LF_{sfc}^{LST} indicates the suppression of thermal emission after the land conversion or, expressed differently, less longwave radiation dissipated from the converted surface attributable to its lowered LST. This suppression also decreases both the longwave radiation absorbed by the atmosphere and that escaping at the TOA. Globally, only an average of 22 W/m^2 surface emission out of 390 W/m^2 (~5.6%) escapes into space (Costa and Shine 2012), a value lower than the previous estimate of 40 W/m^2 (~10%) by Trenberth et al. (2009). This global-scale partitioning provides ratios to roughly apportion surface longwave forcing LF_{sfc} into longwave RFs at the TOA and for the atmosphere as follows:

$$LF_{toa}^{LST} = 22/390 \times LF_{sfc}^{LST}$$

$$LF_{atm}^{LST} = -368/390 \times LF_{sfc}^{LST} \quad (7)$$

where the "minus" sign in the apportioning for LF_{atm} ensures that a positive LF value means that the system gains more longwave radiation or loses less radiation compared to the original vegetation. In our analyses of the four classes of vegetation replacement, LST and downward longwave flux as used in Eq. 6 are obtained from the MODIS daytime and nighttime LSTs and the

CERES longwave flux product, respectively. Surface emissivity is estimated from albedo using an empirical relationship developed by Juang et al. (2007), $\varepsilon = 0.99 - 0.16\alpha_{sfc}$.

The second type of longwave RF is caused by the change in atmospheric water vapor concentration due to altered ET. Different from the albedo-induced RF of Eq. 3 or the LST-induced longwave RF of Eq. 6, this type of RF is not necessarily confined to locations where ET is altered, attributable to the dynamic nature of atmospheric water vapor transport, which makes its computation difficult. To provide rough estimates for ET-induced longwave RF only, we considered an extreme case assuming that the water vapor is well mixed at the global scale. This assumption allows us to calculate this RF, LF_{toa}^{ET}, for a given time t in a way similar to that of CO_2, but with a different forcing parameter of 20.7 W/m^2, as follows:

$$LF_{toa}^{ET}(t) = 20.7\log\left(1 + \frac{s_{lcc} \times \Delta m_{H2O}(t)}{M_{H2O}}\right) \times \frac{S_E}{s_{lcc}} = 0.83 \times \Delta m_{H2O}(t) \quad (8)$$

where M_{H2O} is the total mass of water vapor in the troposphere, taken simply as 1.27×10^{16} kg; s_{lcc} and S_E again are the respective areas of the converted land and the Earth; the value of 20.7 for the forcing parameter is derived from the simulation results of Collins et al. (2006); and Δm_{H2O} (kg/m^2) is the cumulative change in the atmospheric water vapor at time t contributed by the altered ET input per unit area. This water vapor change is estimated by assuming a mean residence time of 10 days for water vapor:

$$\Delta m_{H2O} = \int_0^t \Delta ET(\tau) \times \exp\left[-\frac{(t-\tau)}{10}\right] d\tau \quad (9)$$

where the change in ET at a given time τ (day) for a land conversion, $\Delta ET(\tau)$ (kg $H_2O \cdot m^{-2} \cdot d^{-1}$; hereafter expressed as $kg \cdot m^{-2} \cdot d^{-1}$), is obtained from the MODIS ET comparison based on adjacent sites. In Eq. 8, S_E/s_{lcc} is applied to transform the global mean ET-induced longwave forcing (i.e., $20.7 \cdot \log(1 + s_{lcc} \cdot \Delta m_{H2O}(t)/M_{H2O})$) to its effective local value LF_{toa}^{ET} to be comparable to the local shortwave RF SF_{toa}. Our estimate of LF_{toa}^{ET} is approximate; we have not attempted to translate this ET-induced longwave forcing into an equivalent C emission.

Non-radiative forcings and re-partitioning of surface energy associated with land conversion

Non-radiative forcings associated with changes in biophysical properties, such as surface roughness, canopy conductance, canopy structure, and rooting depth, also affect temperature. We examined the local impact of these forcings at the surface through the redistribution of sensible (H) and latent ($\lambda \cdot ET$) heat (Fig. 2). In our monthly or annual analyses, the downward energy flux into the ground is typically small; thus, the surface energy balance equation becomes $R_n = H + \lambda \cdot ET$ or $\Delta R_n = \Delta H + \lambda \cdot \Delta ET$. Here, ΔR_n represents the change in surface net radiation after land conversion, and it is dominated by LST- and albedo-induced RFs, $\Delta R_n = SF_{sfc} + LF_{sfc}^{LST}$, because the contributions of ET- and CO_2-induced longwave RFs to the local energy balance are close to zero. The change in latent heat flux $\lambda \cdot \Delta ET$ was obtained from the adjacent comparisons of MODIS ET using the heat of vaporization λ as the conversion factor. Then, the change in sensible heat flux ΔH was estimated as

$$\Delta H = SF_{sfc} + LF_{sfc}^{LST} - \lambda \cdot \Delta ET. \quad (10)$$

Because the warming of near-surface air is fueled directly by sensible heat, we expect that a land conversion with increased sensible heat ($\Delta H > 0$), regardless of the signs of ΔR_n and ΔET, would tend to warm the planetary boundary layer locally and that conversely, a conversion with a negative ΔH would tend to cool the near-surface air locally. For example, an increase of 1 W/m^2 in the sensible flux for a heating cycle of 12 h raises the temperature of a 250-m mixed layer by as much as 0.14 K, which is estimated approximately according to the simple formula of West et al. (2011). In contrast, enhanced latent heat (i.e., $\lambda \cdot \Delta ET > 0$) does not immediately warm the near-surface air, even though this extra energy will be turned into sensible heat somewhere in the upper air, when condensing, and thus, will modify the energy balance of the atmosphere overall. This extra latent heat impacts the local or regional surface energy balances through indirect pathways, such as the greenhouse effect of the associated water vapor and the attenuation of sunlight if the water vapor condenses into cloud droplets. Such interactions are difficult to track directly from MODIS data. Rather, we referred mainly to ET-induced longwave RFs as a metric for assessing the potential impacts of altered ET on regional and global temperature.

The direct heating or cooling of the local atmospheric column above a disturbed land area is determined by both RF $RF_{atm} = SF_{atm} + LF_{atm}$ and non-radiative forcing ΔH. Unlike the change in sensible flux ΔH, the atmospheric radiative forcing RF_{atm} affects temperature throughout the air column, with the maximum influence expected to occur in the middle layer, although the exact altitude depends on the atmospheric opacity at the respective spectral bands. Therefore, the direct effects of the atmospheric RFs SF_{atm} and LF_{atm} on the near-surface air temperature are negligible compared to the non-radiative forcing ΔH.

Results

Albedo

Latitudinal and seasonal variations in albedo resembled changes in snow-water equivalent (Appendix: Figs. A2 and A3), implying the critical role of snow in determining surface albedo (Figs. 3 and 4). Lands

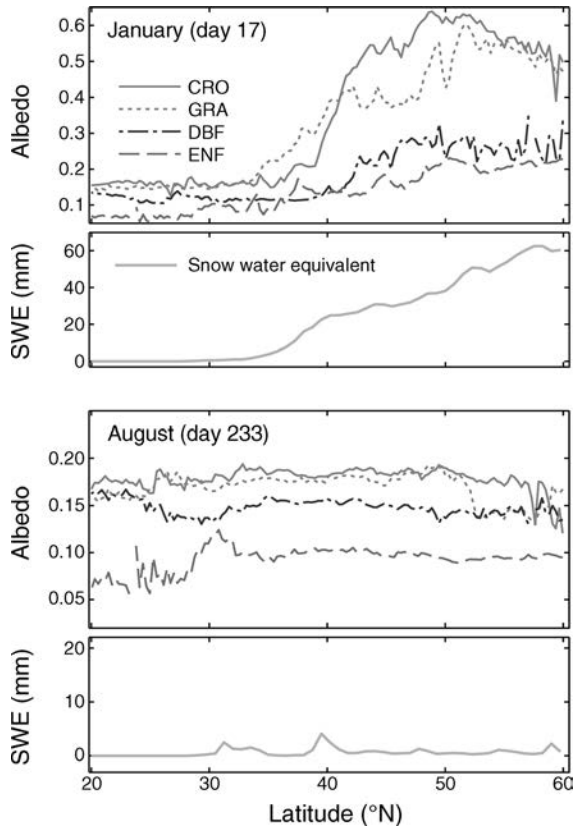

FIG. 3. Comparisons of zonally averaged MODIS white-sky albedo among four land-cover types, including grassland (GRA), cropland (CRO), evergreen needleleaf forest (ENF), and deciduous broadleaf forest (DBF), along the latitude range of 20°–60° N for a winter (top) and a summer (bottom) around day of the year 17 and 233, respectively. The zonal averaging was performed using a 0.1°-latitude bin for zones with more than five MODIS pixels of a vegetation class. For comparison, the associated advanced microwave scanning radiometer-EOS (AMSR-E) snow water equivalent (SWE) is also depicted. Note the different *y*-axis scales in January vs. August.

covered with herbaceous plants or short vegetation normally had brighter surfaces than lands with woody vegetation throughout the year, especially when snow is present (Fig. 5). The zonally averaged MODIS white-sky albedo over 45°–60° N around day of year 17 in January, for example, was 0.57 ± 0.05, 0.50 ± 0.07, 0.26 ± 0.04, and 0.20 ± 0.02 (mean ± SE) for CRO, GRA, DBF, and ENF, respectively. Unlike multilayered forest canopies, croplands and grasslands, which are covered with little or no low-lying live or dead biomass in winter, are more likely to be buried under snow. Foliage losses in deciduous forests exposed more snow-covered ground than in evergreen forests, enhancing the observed wintertime albedo of DBF somewhat compared to ENF (Figs. 3 and 4).

Paired local comparisons of adjacent vegetation types show consistent differences in albedo (Fig. 5). Albedos of CRO and GRA were, on average, greater than those of ENF and DBF. For instance, albedos of GRA and ENF differed by 0.21 in January and 0.054 in July when averaged over paired sites ($P < 0.001$, $n = 317\,911$ paired sites), representing an increase of 97% and 51%, respectively. Croplands generally had albedo values similar to those of adjacent grasslands, although croplands on average were slightly brighter (i.e., an annual mean albedo of 0.216 vs. 0.211 averaged over all the CRO–GRA sites, $P < 0.0001$, $n = 2\,037\,020$). At most of the paired sites, ENF had lower albedo than DBF throughout the year (i.e., annual mean albedo of 0.138 vs. 0.166, $P < 0.0001$, $n = 103\,766$); thus, of the two forest types, DBF tended to have albedo closer to that of CRO or GRA. Another observed pattern was that the four types of vegetated surfaces in temperate regions, especially DBF, all showed a gradual increase in albedo at the beginning of snow-free seasons, and then a gradual decline before snowfall in autumn (Fig. 4). This pattern is driven primarily by seasonal foliage dynamics.

The magnitude of albedo differences between adjacent vegetation types varied with location, as indicated in the results from the *k*-means clustering (Fig. 6). The resultant clusters correspond to distinct geographic regions and were determined mainly by wintertime albedo, reflecting the differing regimes of snow and vegetation interactions across regions. For example, the three clusters of the DBF–CRO sites occupied distinct latitudinal bands in the Eastern USA (Fig. 6); thus, latitude can serve as a proxy to explain the observed pattern in albedo difference between DBF and CRO. As another example, the difference in annual albedo between CRO and GRA was 0.005 ($P < 0.001$) when averaged over all the paired CRO–GRA sites, compared to those of −0.0007 ($P = 0.012$), 0.02 ($P < 0.001$), and −0.036 ($P < 0.001$) when averaged separately over the three clusters (Fig. 6): This spatial pattern suggests some differences in wintertime standing biomass of grasses and crops across regions, which affect albedo dynamics of snow-covered surfaces and are caused in part by differences in crop types and management practice. The pattern may also be influenced by the spatial variation in amount and length of snow cover.

Land surface temperature (LST)

The seasonal and latitudinal variations of land surface temperature (LST) were determined by both the incoming TOA solar radiation and land surface characteristics. The percentages of spatiotemporal variations in LST explained by the TOA solar radiation were 79.4%, 82.8%, 67.2%, and 82.6% for ENF, DBF, GRA, and CRO, respectively (Appendix: Fig. A4). The unexplained variations partially underscore the effects of surface characteristics on LST. In terms of zonally averaged summertime LST, GRA often appeared to be the warmest, followed by CRO, ENF, and DBF. For example, at 35° N, GRA surfaces were ~5.0 K warmer than ENF in July. Our paired local comparisons further reveal the apparent controls of vegetation on LST (see Fig. 7). In terms of daily LST, forested surfaces were

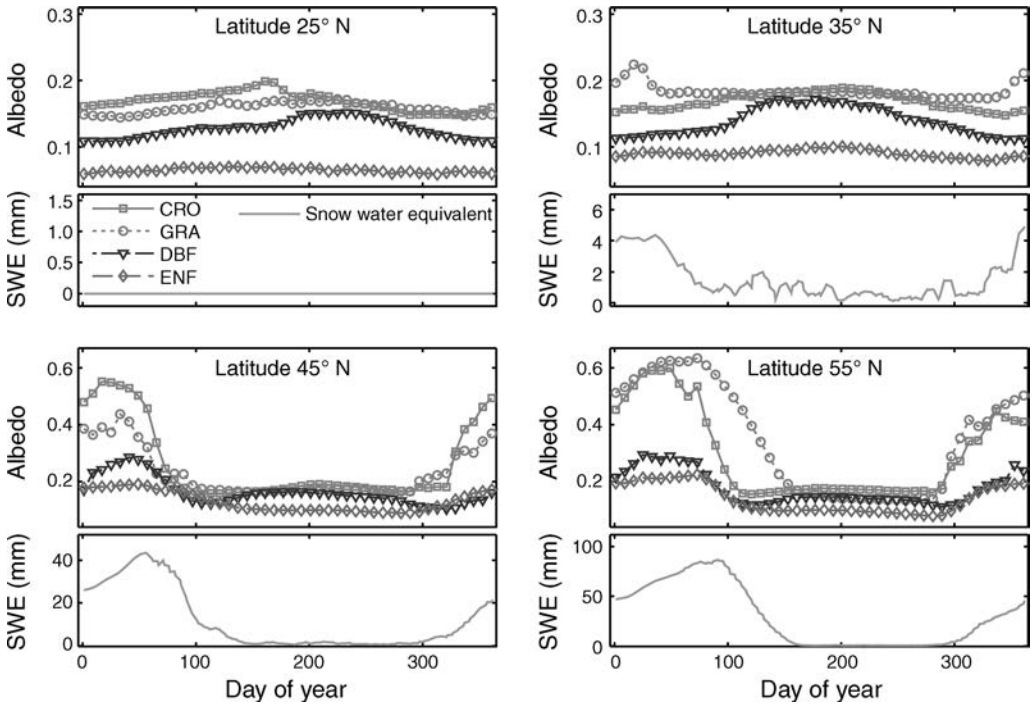

FIG. 4. Seasonal variations in zonally averaged MODIS albedo for four vegetation types, including grassland (GRA), cropland (CRO), evergreen needleleaf (ENF), and deciduous broadleaf forest (DBF), at selected latitudes: 25° N, 35° N, 45° N, and 55° N. The zonal averaging was performed over the 0.1°-latitude bin centered at each selected latitude. The associated AMSR-E snow water equivalent (SWE) is also presented. Note that the scales for *y*-axes vary for better visualization.

cooler in warm seasons, but warmer in cold seasons than adjacent GRA and CRO lands (Fig. 7). Surfaces of GRA were, on average, slightly warmer than adjacent CRO, especially in summer (i.e., 301.2 K vs. 299.1 K in the June–August mean daily LST, $P < 0.0001$, $n = 151\,644$); therefore, during warm seasons, the warming of GRA surface relative to adjacent forests was more pronounced than that of CRO to forests.

The examination of daytime and nighttime LST suggests a diurnal asymmetry in temperature differences (Fig. 7). Daytime LST of CRO or GRA compared to adjacent forests was markedly higher during warm seasons, but was similar or slightly lower during cold seasons. For instance, the difference in daytime LST between CRO and ENF was 6.4 K in July, but −0.046 K in January averaged across all paired sites ($n = 10\,105$). In contrast, nighttime LST of CRO or GRA was consistently lower than adjacent forests throughout the year (i.e., a mean annual nighttime LST difference of −0.28 K between CRO and ENF; Fig. 7). This diurnal LST asymmetry indicates that the patterns of differences in daily LST between non-forest and forest types were dominated by differences in daytime LST during the warm seasons and by nighttime LST during the cold seasons.

Additionally, our paired comparisons between adjacent vegetation illustrate clear patterns in daily temperature range (DTR), defined as the difference between MODIS-observed daytime and nighttime LSTs. For a given vegetation type, DTR during the warm seasons was larger than during the cold seasons (Fig. 8). In most cases, ENF and DBF had smaller DTRs than adjacent GRA and CRO sites, with an annual DTR of 3.98 K and 5.23 K for DBF and CRO ($n = 23\,544$), respectively (Fig. 8). The DTR values, however, likely underestimate the true values because satellites rarely measure extreme temperatures due to insufficient temporal resolutions.

Evapotranspiration

Our large-scale analyses of zonally averaged ET clearly revealed the controls of vegetation on surface water fluxes (Appendix: Fig. A5). Among the four vegetation types, deciduous forests annually evaporated the most water, and grasslands generally evaporated the least water. When spatially averaged over our study area, the mean annual ET for DBF, ENF, CRO, and GRA was 1.61, 1.36, 1.42, and 0.98 $kg{\cdot}m^{-2}{\cdot}d^{-1}$, respectively, with DBF evaporating an average of 18% more water than ENF; the mean summertime ET for DBF, ENF, CRO, and GRA was 2.86, 2.01, 2.19, and 1.32 $kg{\cdot}m^{-2}{\cdot}d^{-1}$, respectively. Although the spatially averaged annual ET of CRO was larger that of ENF, their relative magnitudes depended on latitude and season. For example, over 20°–30° N, the annual ET of ENF and CRO averaged 1.84 and 1.78 $kg{\cdot}m^{-2}{\cdot}d^{-1}$, with ENF evaporating slightly more water than CRO. Seasonal ET variations are synchronous with growth seasons (Appendix: Fig. A5), and the overall latitudinal

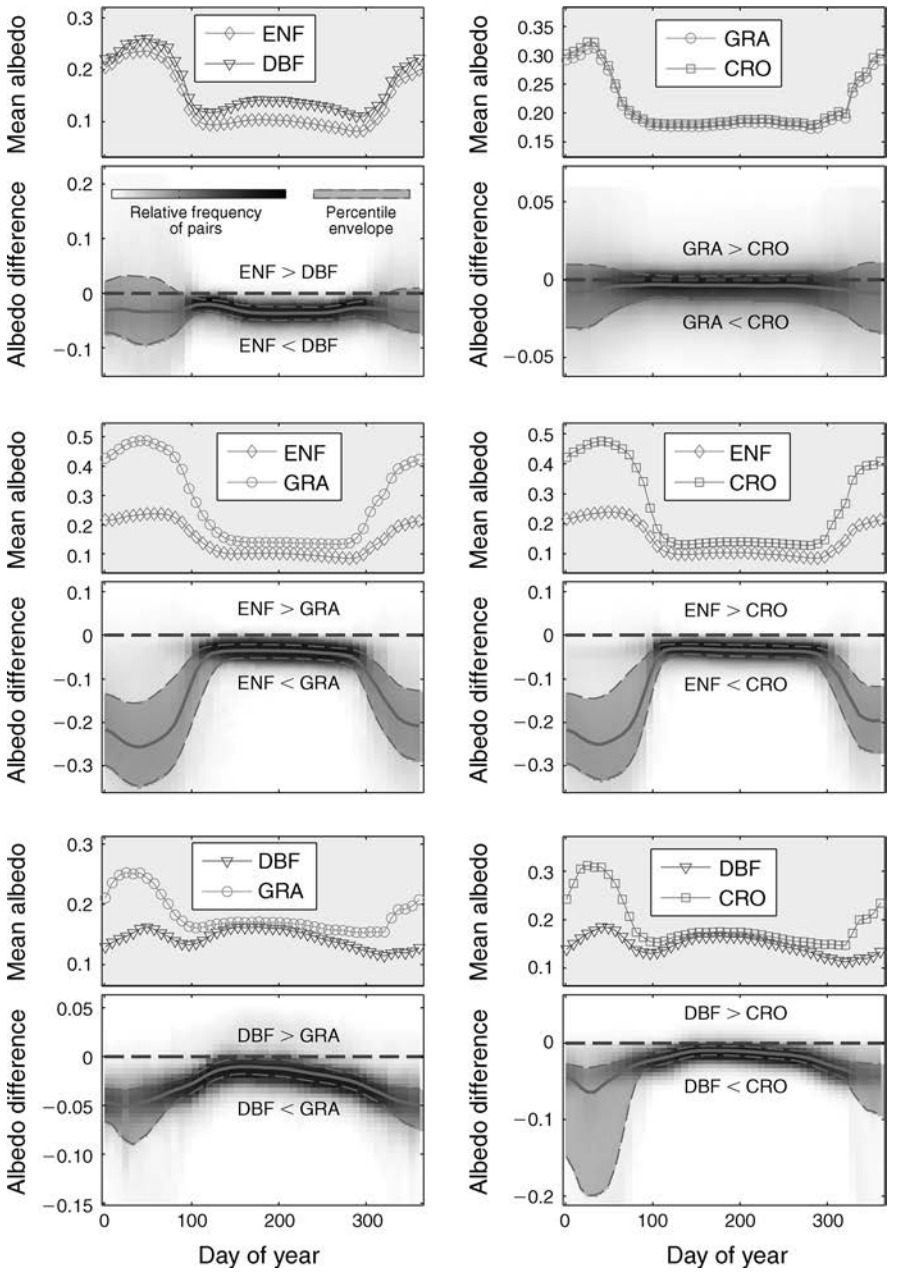

FIG. 5. Comparisons of MODIS albedo between spatially adjacent vegetation types. For each pair of vegetation types (e.g., DBF vs. CRO on the lower right), the upper part depicts the mean albedo averaged over all the paired sites; the lower part shows distributions of albedo difference between the two vegetation types on each observation date throughout a year. The distribution for each date represents the relative number of sites that have a given value of albedo difference on that date and, for ease of display, is depicted in a grayscale scheme: Darker color suggests a larger number of sites. The solid curve enveloped in gray denotes the medians of albedo difference as a function of date; and the two dashed lines confining the envelope indicate the upper and lower 25% percentiles. The sites chosen in each comparison were identified across North America as locations where pixels of the two contrasting vegetation types co-occur within a 30-km window. Note that the scales for *y*-axes vary for better visualization.

dependence of ET is linked to a shortening of growth period at high latitude.

Paired comparisons based on adjacent sites further revealed the effects of vegetation on surface water fluxes (Table 2, Fig. 9). Overall, the results were consistent with those from the large-scale comparison, though not identical. In particular, DBF evaporated more water than adjacent ENF. For example, averaged over the paired DBF–ENF sites, ET of DBF and ENF in July was 3.30 and 2.69 $kg \cdot m^{-2} \cdot d^{-1}$, representing a 22% increase for DBF relative to ENF ($P < 0.001$, $n = 29\,390$). Of the two non-forest types, CRO, on average,

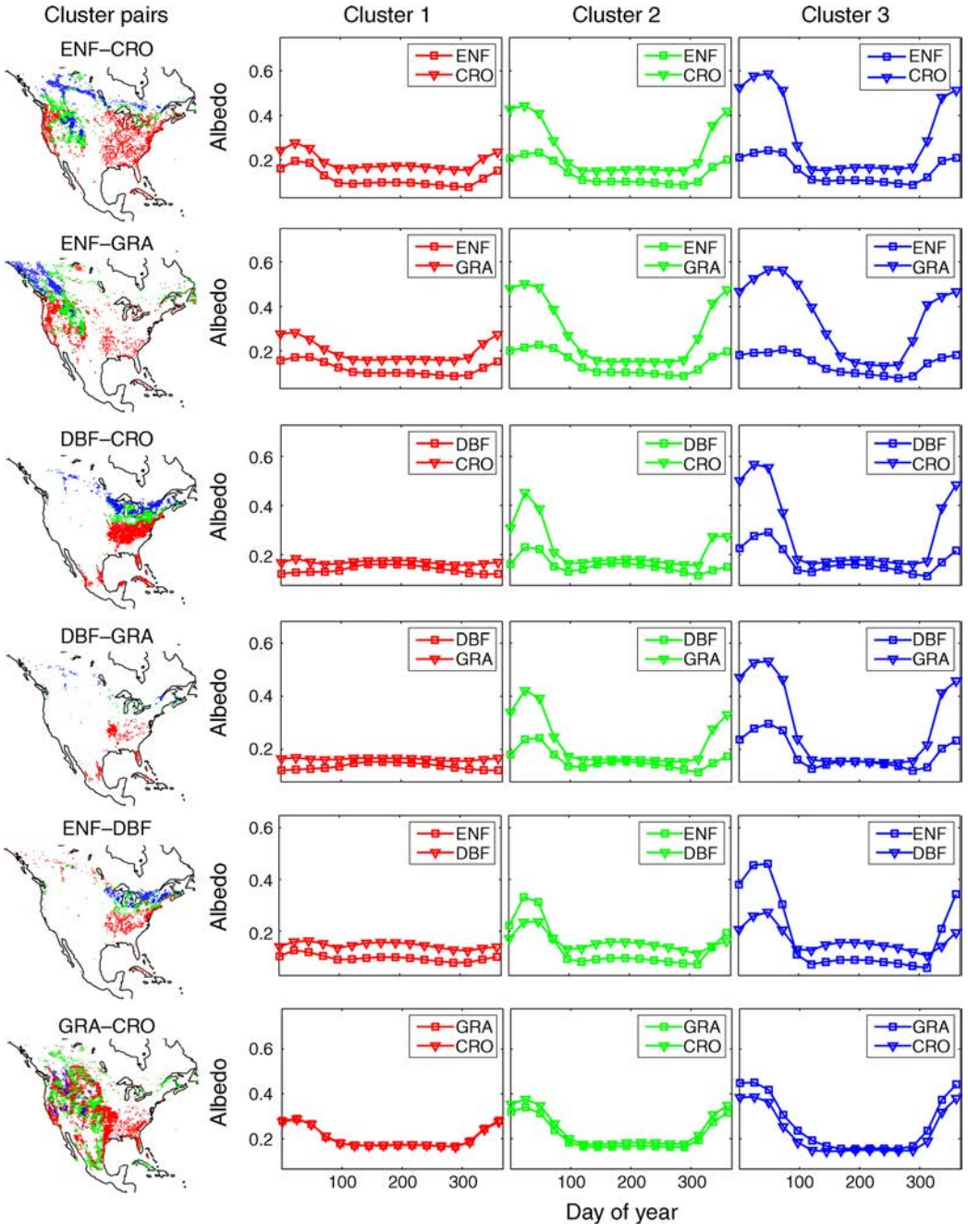

FIG. 6. A further analysis, as in Fig. 5, comparing albedo between matched adjacent sites of contrasting land covers. The sites, where a pair of land covers is co-located nearby, were subdivided by the *k*-means clustering algorithm into three distinct clusters according to seasonal patterns of albedo difference. For each pair of vegetation classes, the geographic distributions of the three resultant clusters are mapped in color (the leftmost of each row), and the mean albedos averaged over all the sites of each cluster are also displayed (the three plots on the right in the same color respectively).

evaporated more water than adjacent GRA during the growing season (e.g., 2.36 vs. 2.26 $kg \cdot m^{-2} \cdot d^{-1}$ in July, $P < 0.001$, $n = 225\,904$), but annually, the average ET of CRO was slightly smaller than that of GRA (e.g., 1.28 vs. 1.33 $kg \cdot m^{-2} \cdot d^{-1}$, $P < 0.001$). In winter or dormant seasons, ET differences were marginal between DBF and ENF or between CRO and GRA, partly because ET remained low in all cases.

Forests were found to generally evaporate more water than adjacent non-forest vegetation (Fig. 9). When averaged over all paired sites, ENF annually evaporated slightly more water than did CRO (i.e., 1.32 vs. 1.25

$kg \cdot m^{-2} \cdot d^{-1}$ for ENF and CRO, $P < 0.001$, $n = 28\,547$); DBF evaporated 0.25 kg/m^2 more water per day than CRO over the year (i.e., 1.79 vs. 1.54 $kg \cdot m^{-2} \cdot d^{-1}$ for DBF and CRO, $P < 0.001$, $n = 18\,223$). On average, forests also showed higher annual ET than did adjacent grasslands (Fig. 9), although the differences were small; for example, the annual ET averaged over the paired DBF–GRA sites were 1.71 and 1.67 $kg \cdot m^{-2} \cdot d^{-1}$ for DBF and GRA ($P < 0.001$, $n = 19\,216$), respectively. In addition, the ET differences between adjacent non-forest and forest sites also showed some spatial and temporal variability (Fig. 9; Appendix: Fig. A6), reflecting multiple controls on ET such as climate, variations in crop/grass phenology, and land management practices. The partitioning of surface energy for CRO was greatly influenced by crop type and the timing of planting and harvesting. Many croplands with high annual ET, as delineated by the *k*-means clustering (Appendix: Fig. A6), coincided roughly with the irrigated areas derived by Pervez and Brown (2010), again emphasizing the influences of crop management. Moreover, these mixed results may be affected by uncertainties in the MODIS ET products.

Atmospheric regulation of albedo effect

The analysis of the CERES data highlights that RF from land-use change is determined not just by the magnitude of surface albedo change, but also by atmospheric conditions. This observation arises in part from atmospheric attenuation of upwelling surface reflection, thereby diminishing the surface contribution to the TOA albedo. The annual TOA albedo over our study area averaged 0.32, with a contribution of 0.28 from the atmosphere and only 0.04 from the land surface. The surface contribution represented only ~29.5% of the actual surface albedo. Moreover, the fraction of surface contribution to TOA albedo was negatively correlated to the amount of clouds, with an estimated coefficient of −0.82 ($P < 0.001$) over North America (Appendix: Fig. A7). This correlation indicates that the atmospheric opacity, as determined largely by cloudiness, exerts additional controls on the observed change in TOA albedo and, correspondingly, on the magnitude of RF associated with land conversion. All else being equal, the TOA RF from land albedo reduction is larger in less cloudy areas. Thus, the same reduction in surface albedo will lead to a stronger warming for reforestation and afforestation in the USA west of 95° W, where the cloud fraction and the fraction of surface contribution to TOA albedo averaged 47.7% and 20.3%, respectively, compared to the eastern half of USA, where the two fractions averaged 62.0% and 10.9%.

Shortwave RF and carbon emission equivalent

The conversions from CRO or GRA to DBF generally yielded smaller RFs than did the conversions to ENF (Table 2), as expected from the observed albedo differences between adjacent vegetation types (Fig. 5). When averaged over the common locations where the conversions of CRO to ENF and DBF are both possible (i.e., "triplets"), primarily in the eastern USA, the TOA shortwave RF was estimated to be 7.55 W/m^2 for the CRO–ENF conversion, almost twice the value of 3.87 W/m^2 for CRO–DBF. Moreover, a strong spatial dependence was evident in the TOA RF induced by the non-forest to forest transitions, as determined by spatial patterns in albedo difference and atmospheric opacity (Fig. 10; Appendix: Fig. A5). Large RFs were more frequently observed at more northern latitudes or in the western USA, but the overall latitudinal dependence was weak. The control of the atmosphere on RF was revealed such that many regions yielding large RFs coincided with areas that have large fractions of surface contributions to TOA albedo or small atmospheric attenuation, especially over the Rocky Mountains (Fig. 10). Correlations between RFs and the fractions of surface contribution to TOA albedo were substantial, for example being 0.48 ($P < 0.001$) and 0.52 ($P < 0.001$) for the CRO–ENF and the CRO–DBF conversions, respectively.

In addition to its distinct spatial pattern, albedo-induced shortwave RF exhibited some characteristics that differ from those of CO_2-induced RF. In particular, the magnitude of albedo-induced RF was always larger at the surface than at the TOA (i.e., $SF_{sfc} > SF_{toa}$). This result is also revealed from the relationship $SF_{sfc} = SF_{toa} - SF_{atm}$, where $SF_{atm} < 0$ for reduced surface albedo, because less solar energy will be reflected upward to radiatively heat the atmosphere. For example, the estimated annual mean shortwave RFs for the CRO–ENF conversion were 8.45 W/m^2, 6.11 W/m^2, and −2.33 W/m^2 at the surface, TOA, and for the atmosphere, respectively. The surface RF SF_{sfc} does not necessarily increase the surface temperature because this energy (e.g., 8.45 W/m^2) is further re-partitioned; in contrast, the atmospheric RF forcing SF_{atm} (e.g., −2.33 W/m^2) directly cools the atmospheric column. On average (±SD), about 27.6% ± 3.0% of the surface RF was derived from the loss of radiation absorbed by the atmosphere, but the exact value for this ratio varied with scale (~29.2% at the monthly scale). Both the values of 27.6% and 29.2% appeared close to but slightly higher than 23% as used by Montenegro et al. (2009). In addition, the geographic patterns of surface RF were observed to be similar to those of TOA RF; therefore, the conversion to DBF generally had smaller surface RF than that to ENF.

Conversions of non-forest vegetation, GRA or CRO, to DBF usually had considerably smaller carbon emission equivalents than conversions to ENF had. Carbon emission equivalents, δC_{alb}, were obtained by multiplying TOA shortwave RFs by a factor of 0.312 (kg/W). By doing so, the global longwave RF induced by this carbon emission is equivalent to the local albedo-induced shortwave RF when spread over the globe in

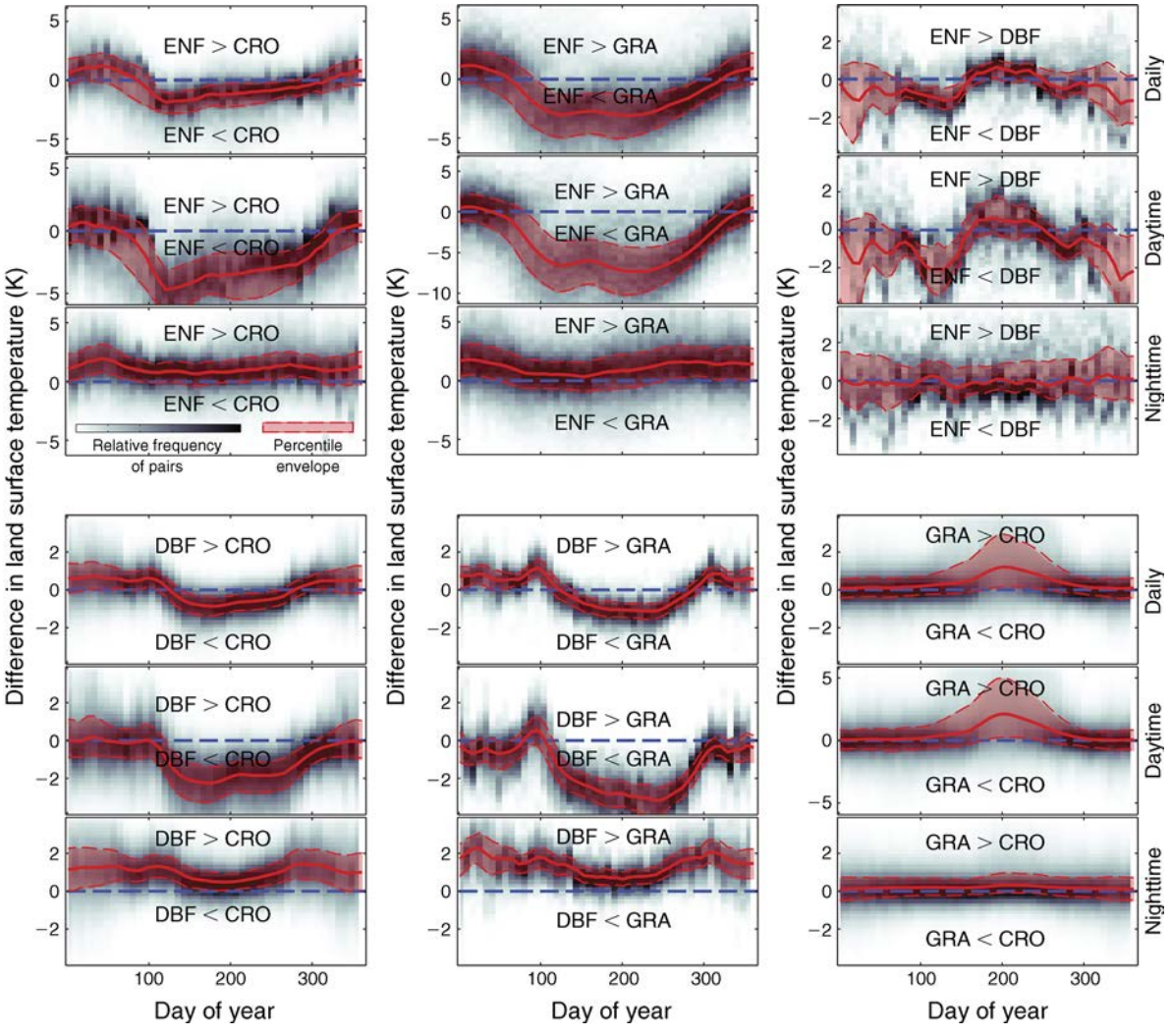

FIG. 7. Comparisons of MODIS land surface temperature (LST) between adjacent sites of contrasting vegetation for six pairs of vegetation types (e.g., ENF vs. CRO and ENF vs. GRA). For each pair of vegetation types, the upper, middle, and bottom panels of each subfigure refer to differences in daily, daytime, and nighttime temperature, respectively. The gray color scheme indicates the distribution of LST differences for each date, which is the relative number of sites that have a given value of LST difference on that date; darker color suggests a larger number of sites. The red solid curves denote the medians of LST difference as a function of date; the dashed lines indicate the upper and lower 25% percentiles of LST differences between the paired vegetation types. The units for LST are in degrees Kelvin (K).

terms of temperature response (see Eq. 4 or Fig. 2). As a result, the spatial patterns of carbon-emission equivalents are the same as those of TOA RFs (Fig. 10). The mean carbon-emission equivalents over the lands bounded by (95°–70° W) × (20°–45° N) were estimated to be 2.1 ± 0.4 kg/m^2 (CRO–ENF), 0.87 ± 0.47 kg/m^2 (CRO–DBF), 2.1 ± 0.5 kg/m^2 (GRA–ENF), and 0.82 ± 0.34 kg/m^2 (GRA–DBF), for the four land conversions, respectively. These values are smaller than the previously reported estimation (Betts 2000), due partly to our correction for the difference in climate sensitivity between CO_2- and albedo-induced RFs (see Eq. 4 or Fig. 2).

The net carbon drawdown, $\delta C_{seq-alb}$, for land conversions from CRO or GRA to forests in our study area was in most cases positive, suggesting that the combined effect of reduced albedo and CO_2 uptake on global temperature is cooling. Previous estimates of carbon sequestration potential of forestry projects in our study area fall within the range of 5.5–18 kg C/m^2 (Betts 2000, Claussen et al. 2001, Gibbard et al. 2005, Montenegro et al. 2009). These estimates of δC_{seq} are larger than our estimated carbon emission equivalent to albedo-induced RFs δC_{alb}, resulting in positive values of net carbon drawdown $\delta C_{seq-alb}$. Even if forests drawn down additional carbon by only 5.5 kg C/m^2 in their below- and aboveground pools, the carbon emission

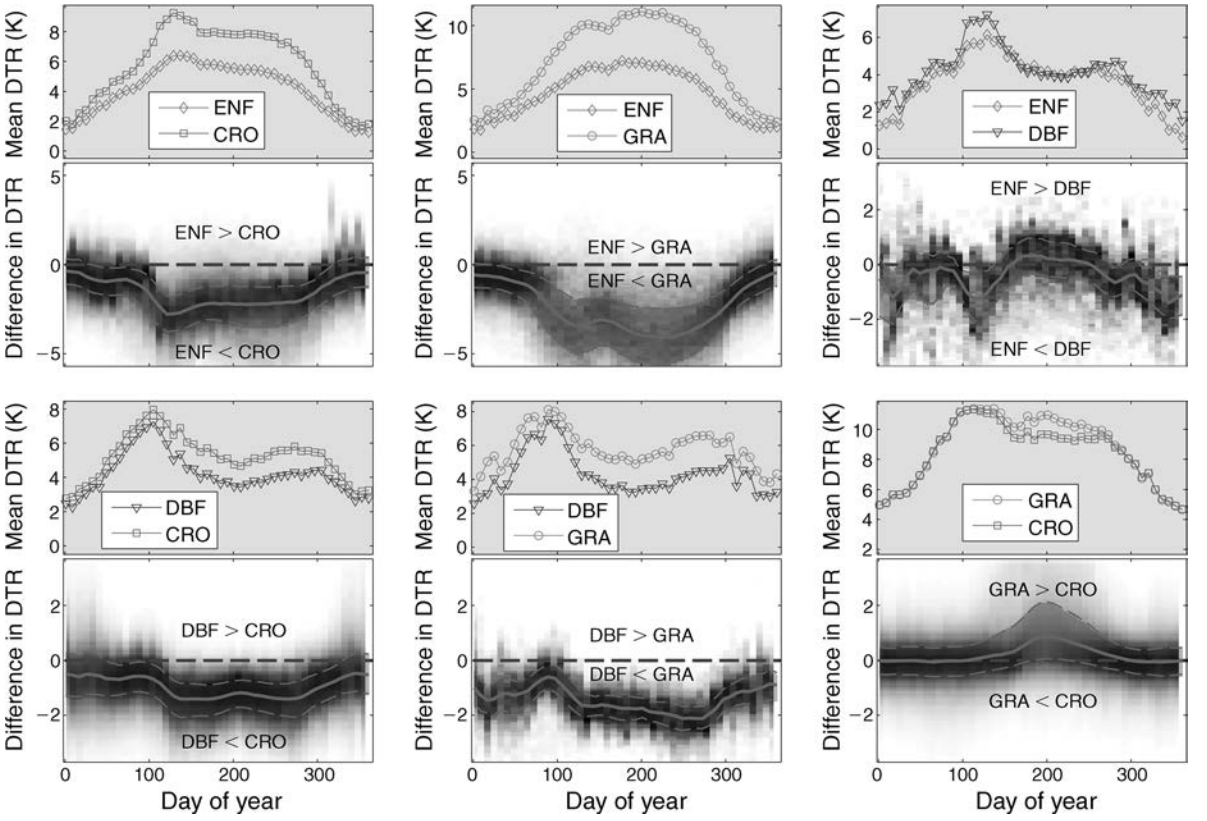

FIG. 8. Comparisons of daily surface temperature range (DTR) between matched adjacent sites of contrasting vegetation for six pairs of vegetation classes. In each subfigure, the upper panel refers to mean DTR and the bottom refers to the distributions of difference in DTR; that is, the relative number of sites that have a given value of DTR difference. The interpretation of dashed lines and grayscale gradients is the same as in Fig. 5. The units for DTR are in degrees Kelvin (K).

TABLE 2. Changes in surface biophysical properties for potential land conversions from non-forest (croplands [CRO] or grasslands [GRA]) to forest (deciduous forests [DBF] or evergreen forests [ENF]) in North America and the associated biophysical forcings as derived from the combination of multiple satellite observations and products.

Altered biophysics	CRO→DBF	CRO→ENF	GRA→DBF	GRA→ENF
ΔAlbedo	−0.0540 ± 0.035	−0.0841 ± 0.037	−0.0535 ± 0.040	−0.0996 ± 0.050
ΔTOA albedo	−0.0148 ± 0.012	−0.0247 ± 0.012	−0.0148 ± 0.013	−0.0288 ± 0.015
ΔLST	−0.046 ± 0.42	−0.55 ± 1.3	−0.11 ± 0.81	−1.27 ± 1.6
sfc				
SF	4.35 ± 2.1	8.45 ± 2.4	4.18 ± 2.8	9.63 ± 2.9
LF (LST)	0.266 ± 2.3	2.50 ± 6.1	0.67 ± 4.6	6.36 ± 8.3
toa				
SF	3.13 ± 1.6	6.11 ± 1.9	3.01 ± 2.1	7.01 ± 2.2
LF				
LST	0.015 ± 0.13	0.14 ± 0.34	0.038 ± 0.26	0.36 ± 0.47
ET	3.24 ± 2.4	0.016 ± 5.4	1.26 ± 2.1	−0.44 ± 2.3
atm				
SF	−1.23 ± 0.53	−2.33 ± 0.58	−1.17 ± 0.73	−2.61 ± 0.97
LF(LST)	−0.25 ± 2.1	−2.36 ± 5.7	−0.63 ± 4.3	−6.00 ± 7.8
ΔLatent heat	7.36 ± 5.1	0.012 ± 5.2	2.48 ± 5.6	0.029 ± 5.5
ΔSensible heat	−4.82 ± 5.3	10.54 ± 7.0	3.64 ± 7.9	13.59 ± 7.7

Notes: Radiative forcings are reported for both longwave (LF) and shortwave (SF) at the surface (sfc), the top of the atmosphere (toa), or for the atmosphere column (atm). Longwave radiative forcings (LF) can be induced by altered land surface temperature (LST) or evapotranspiration (ET). The values reported here represent the spatial averages and standard deviations (SD) of annual means of each variable across all valid $1^\circ \times 1^\circ$ grids where potential land conversions occur. Note that different sets of grids were used for evaluating different variables. Also note that LST here refers to the average of daytime and nighttime temperatures. Units are K for LST and W/m^2 for other variables except albedo (unitless).

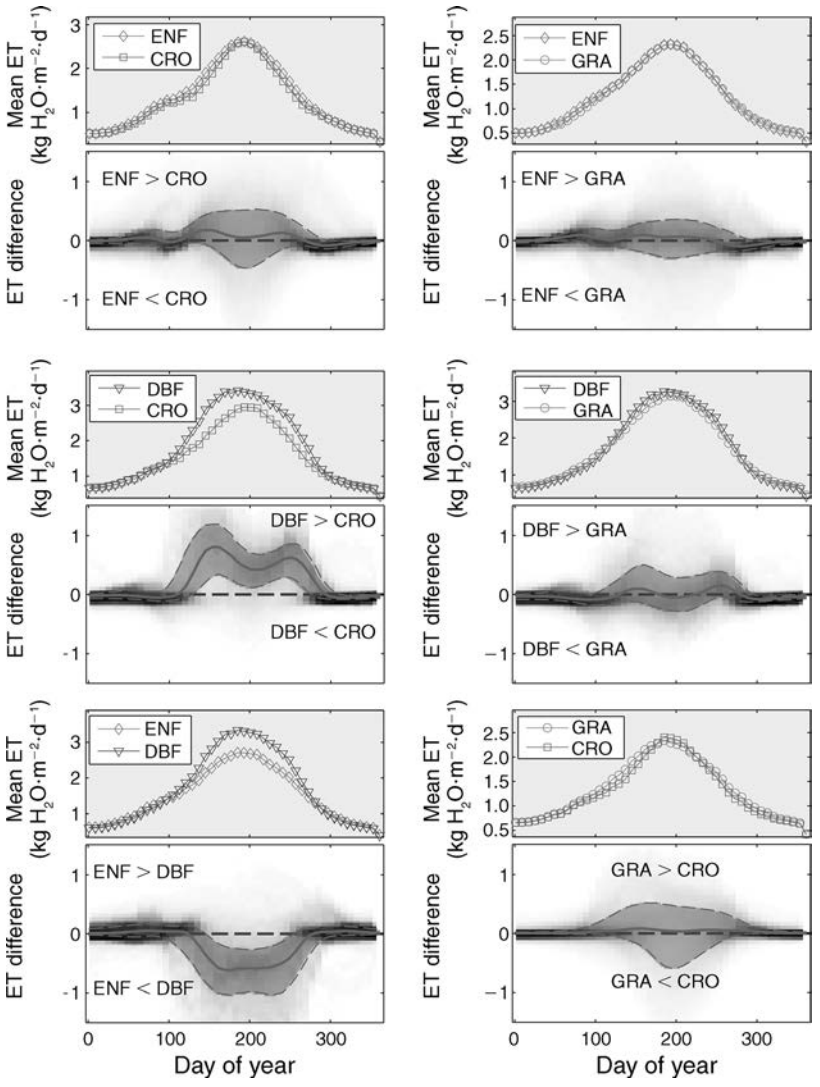

FIG. 9. Comparisons of MODIS evapotranspiration (ET) between contrasting vegetation at adjacent sites. For each of the six pairs of vegetation classes, depicted are the mean ET (upper panel) and the distributions of ET difference between the paired vegetation classes. The distribution for each date is the relative number of sites that have a given value of ET difference (lower panel) and is depicted in a grayscale scheme: A darker color means a larger number of sites. The gray solid curve represents the median value of ET difference; and the dashed lines indicate the upper and lower 25% percentiles. The sites considered for this analysis are locations where both vegetation classes of the pair co-occur within a 30-km window.

equivalent to albedo-induced RF (e.g., an average of 2.2 kg C/m^2 for the conversion of GRA to ENF), is still likely to be counterbalanced. Given the same carbon sequestration potential, the net carbon drawn for DBF is on average larger than that for ENF because the conversions to DBF yielded smaller albedo-induced RFs than did the conversions to ENF. In this case, DBF are more likely to cool globally.

Longwave RF

Annual mean longwave RFs induced by changes in LST (i.e., LF_{sfc}^{LST} and LF_{toa}^{LST}) were found to be smaller in general than the corresponding shortwave RFs SF induced by albedo reduction. This comparison was valid when examined at both the surface and the TOA, although the longwave RF for the atmospheric column LF_{atm}^{LST} sometimes had a larger magnitude than its shortwave counterpart SF_{atm} (Table 2). For example, in the CRO–ENF conversion, the surface forcing LF_{sfc}^{LST} averaged over all paired sites was 2.50 W/m^2, associated with a local atmospheric and TOA longwave RF of –2.36 and 0.14 W/m^2, respectively. This surface longwave RF was more than three times smaller than its shortwave counterpart of 8.45 W/m^2. For the GRA–ENF conversion, the surface longwave RF LF_{sfc}^{LST} became comparable to the shortwave RF SF_{sfc} (i.e., 6.36 W/m^2 for LF vs. 9.63 W/m^2 for SF), leading to a total surface RF of 16.0 W/m^2. Even in this case, the

TOA longwave RF LF_{toa}^{LST} was still marginal compared to the TOA shortwave RF SF_{toa} (i.e., 0.36 vs. 7.01 W/m^2), but the atmosphere column showed a negative longwave forcing LF_{atm}^{LST} of −6.00 W/m^2, larger in magnitude than its shortwave counterpart SF_{atm} of −2.61 W/m^2.

Unlike the LST-induced TOA longwave RF LF_{toa}^{LST}, the TOA longwave forcing induced by altered ET LF_{toa}^{ET} was sometimes comparable to the albedo-induced shortwave TOA RF SF_{toa} (Table 2). For instance, the CRO–DBF conversion produced a mean TOA forcing of 3.24 W/m^2 for LF_{toa}^{ET} and 3.13 W/m^2 for SF_{toa}. As a result, the ET-induced longwave RF might not be negligible, as assumed in many studies. In other words, considering only albedo-induced RF potentially exaggerates the global cooling effect of reforestation and afforestation due to the omission of positive ET-induced longwave RF. Rigorous assessments of biophysical effects of land-use change should therefore carefully examine longwave RFs other than just the albedo-induced shortwave RF.

The relative magnitudes of shortwave and longwave RFs depend not only on location, but also on the time of year examined. For example, the surface longwave RF from altered LST exceeded the associated shortwave RF in certain months, as depicted for the conversion from CRO to DBF in June and July (Fig. 11). Rotenberg and Yakir (2010) also observed that, in a dryland ecosystem, the suppression of thermal emission from forests relative to adjacent open lands yielded an annual mean surface longwave RF slightly larger than the surface shortwave RF induced by albedo reduction.

Re-partitioning of sensible and latent heat

The combination of the surface longwave and shortwave RFs yielded changes in surface net radiation that were found to be mostly positive for conversions to forests (Table 2). The proportion of this positive energy that is dissipated via sensible heat (or more precisely, the ratios of the change in sensible heat to the total RF) varied by land conversion, with medians of 99% (CRO–ENF), 93% (GRA–ENF), 141% (GRA–DBF), and −143% (CRO–DBF) for the four conversion scenarios, respectively. The negative ratio of −143% means that the sensible heat flux after conversion was reduced, with a magnitude larger than the gain in surface net radiation. For example, after converting CRO to DBF, the surface on average gained 2.54 W/m^2 net radiation, but released 4.82 W/m^2 less sensible heat, with the difference attributable to an increase in latent heat by 7.36 W/m^2.

Conversions of CRO or GRA to DBF in many cases led to a negative change in sensible heat flux whereas conversions to ENF led to a positive change (Table 2, Fig. 10). This result is particularly important because it suggests that conversions to DBF are more likely to cause a local cooling to the near-surface air, in contrast to conversions to ENF, which tend to warm the air locally (Fig. 10). The patterns of local cooling or warming manifested spatial and seasonal dependence (Figs. 10 and 11). For example, although the CRO–DBF conversion led, on average, to a local cooling, with a mean reduction of sensible heat by 4.8 W/m^2, there were several spatial clusters (e.g., western North Carolina, Northern Minnesota, North Dakota, and Vermont [USA]) that showed positive changes in sensible heat, though small in magnitude, indicating a possible local warming over these regions after conversion (Fig. 10). Similar to the surface shortwave and longwave RFs, the changes in sensible and latent heat fluxes also varied across timescales and exhibited some pronounced seasonal patterns (Fig. 11).

Discussion

Land-use change affects climate through multiple factors beyond net greenhouse gas concentrations. As shown here, one pathway through which land conversions to forests can warm local and regional climate is to reduce surface albedo and induce positive shortwave RFs. This albedo effect is particularly important at mid or high latitudes through snow-masking because of differences in canopy structure and height (Jackson et al. 2008). The strength of this albedo-induced RF is also determined by abiotic factors such as atmospheric opacity and soil color. Reduced albedo from growing trees can counteract at least some of the cooling benefit of carbon uptake, an observation with policy implications for land and ecosystem management (McAlpine et al. 2010). One example concerns woody-plant invasion that transforms the herbaceous landscapes of grasslands or savannas. The biophysical changes accompanying these transformations, such as albedo and ET, should be realistically evaluated to determine how the biophysical effect may revise the carbon balance effects of woody-plant invasion. As another example, considering the biophysical effects of removing dryland forests resulted in debates about the role of desertification in affecting climate (e.g., Rotenberg and Yakir 2010).

RFs from altered surface albedo and atmospheric CO_2 have different vertical structures and spatial patterns and, thus, different climate sensitivities (Hansen et al. 2005). Previous studies that have assumed the same temperature responses for CO_2- and albedo-induced RFs may have overestimated the albedo-induced global warming of forests by a factor of up to two. In contrast, we believe that our differentiation of climate sensitivity for CO_2- and albedo-induced RFs provides an improvement for quantifying the climate regulation value of land management. However, unlike well-mixed greenhouse gases, land-use change does not have a single, global value of climate sensitivity, which instead depends on the type, location, and extent of land conversion (Gibbard et al. 2005, Brovkin et al. 2006, Pongratz et al. 2009). The value of 0.53 K/[W/m^2] that we used corresponds to the global replacement of forest with grassland as inferred by Davin et al. (2007). This value is only approximate for local-scale vegetation replacement

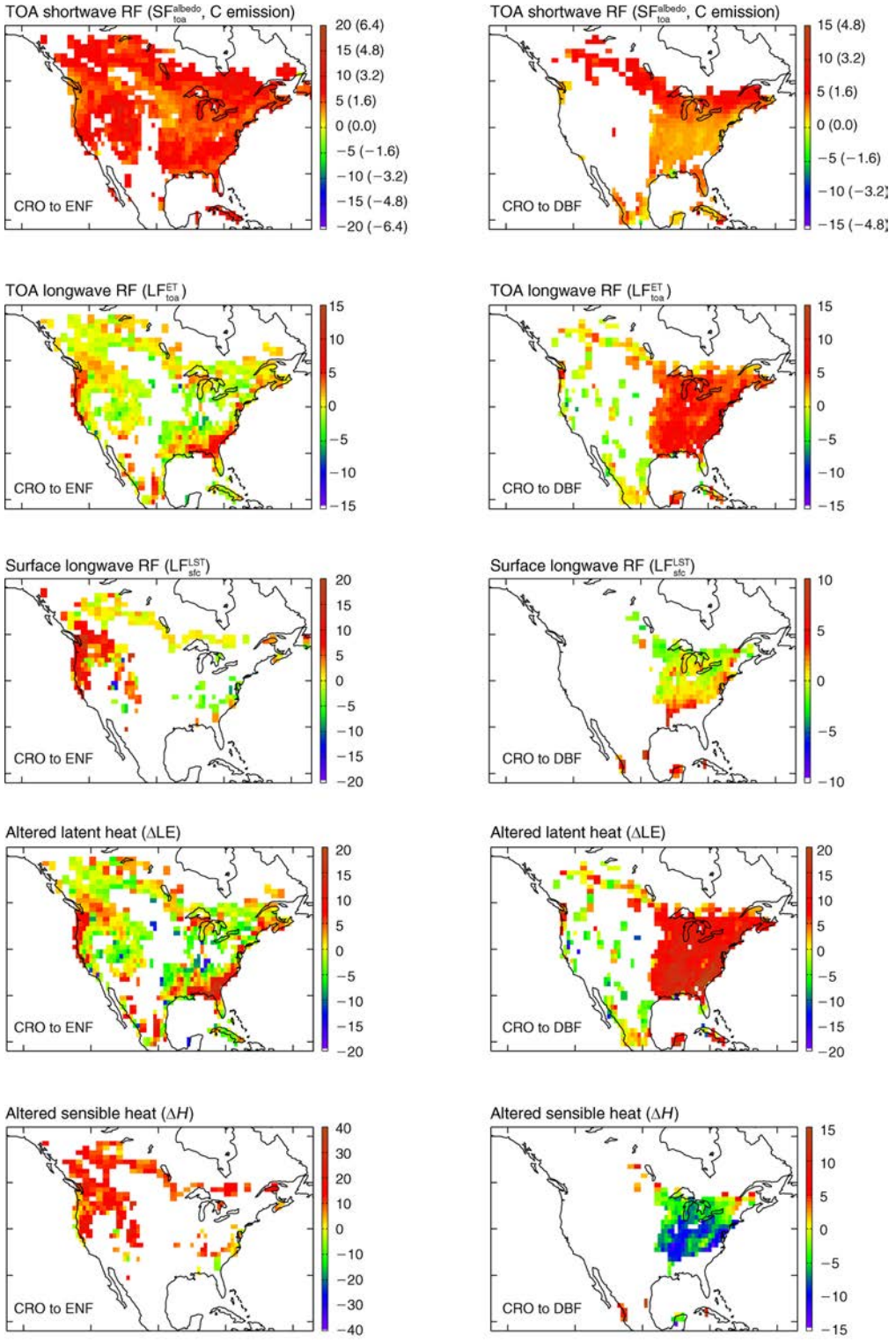

FIG. 10. Spatial patterns in biophysical forcings for land conversions from CRO to ENF (left column) and DBF (right column). Displayed from top to bottom are shortwave radiative forcing (RF) at the top of the atmosphere (TOA) induced by changes in albedo SF^{albedo}_{toa}, with its equivalent carbon emission (values in parentheses), TOA longwave RF induced by altered ET (LF^{ET}_{toa}), surface longwave RF induced by altered LST, changes in latent heat flux (ΔLE), and changes in sensible heat flux (ΔH). The mapped values here represent the annual mean of each forcing at each grid. This analysis considers only those $1° \times 1°$ grids containing at least three MODIS pixels of both vegetation types. Albedo-induced TOA RF was calculated based on MODIS 500-m products and the other forcings were based on 1-km MODIS products, explaining why more valid grids were found for albedo-induced TOA RF than the maps of other forcings. Units are W/m^2 for RF and energy fluxes, and kg C/m^2 for equivalent carbon (values in parentheses).

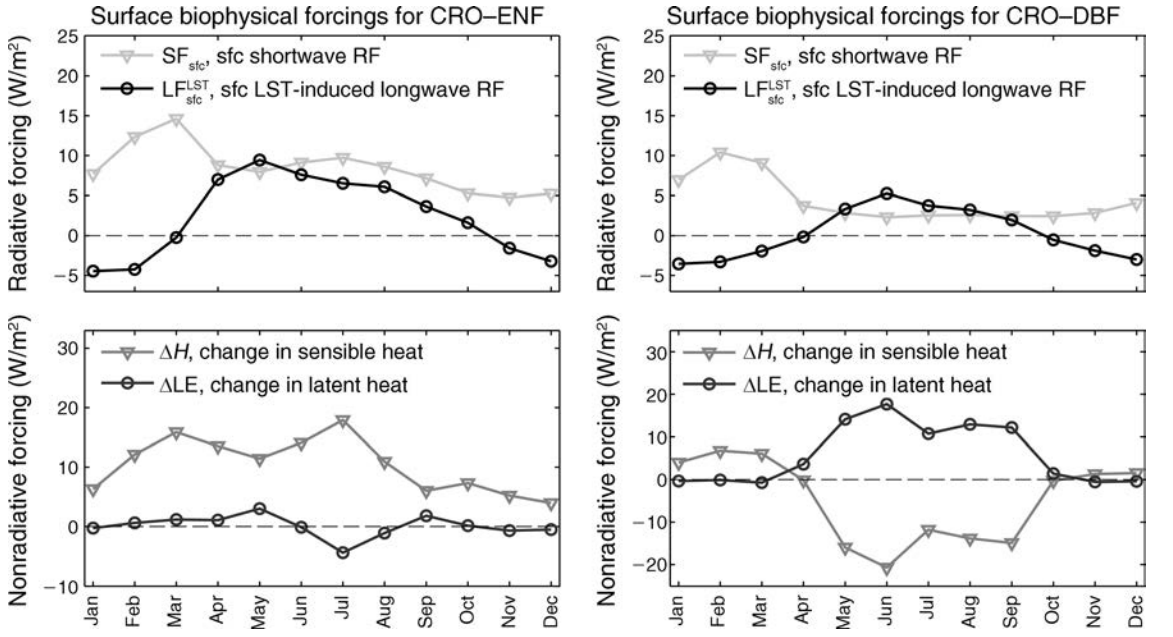

FIG. 11. Seasonal variations in surface (sfc) biophysical forcings for land conversions from CRO to ENF (left) and DBF (right). The radiative forcings (RF) include albedo-induced shortwave RF, longwave RF induced by changed land surface temperature (LST), and changes in sensible and latent heat fluxes, which combine to determine the redistribution of energy at the surface. Values plotted here represent the spatially averaged mean of each forcing at the monthly scale.

in our analyses. A more strict treatment of the disparity in climate sensitivity between the two forcing agents has not, to our knowledge, been adequately explored.

The use of RF for quantifying the climate-regulation services of different land-use practices should also distinguish between different types of forcings to better represent their effects. RFs from different forcing agents often manifest different temporal, spectral, vertical, and spatial characteristics (Bonan 2002, Rotenberg and Yakir 2010). For example, RF for well-mixed greenhouse gases typically refers to the global longwave radiative imbalance once the stratosphere reaches a new equilibrium, but this definition is not applicable to local shortwave RF from small-scale land-use change (National Research Council 2005). Reduced albedo and increased CO_2 both induce positive RFs at the surface and TOA; however, for reduced albedo, the surface RF is larger than the TOA RF, by a factor of ~1.37, whereas for a doubling of CO_2, the surface RF is only ~30% of the TOA RF (Andrews et al. 2009). This contrast in vertical structure further implies that the direct radiative effects in the troposphere will be a cooling for reduced surface albedo but a heating for increased CO_2. Another key distinction between the two forcing agents is on their operating timescales. Biophysical forcings occur with land alterations and will disappear if the lands revert to preconditions; in contrast, RFs from CO_2 emissions are long-lasting because the CO_2 remains in the air for many years. Overall, these differing characteristics make it difficult to implement a universal RF-based metric for all climate change assessments.

As emphasized here, in addition to shortwave RF, longwave RF from vegetation shifts is another important type of biophysical forcing that has been largely ignored in many previous studies. In particular, suppressed surface thermal emissions for cooler forested surfaces lead to a radiative imbalance and could be treated as longwave RF, although others have argued that such suppression is better treated as a feedback (Lee et al. 2011). Nonetheless, this LST-induced surface longwave RF was sometimes comparable in magnitude to the albedo-induced shortwave RF and cannot always be ignored for evaluating net surface radiation. However, this LST-induced longwave RF is always small at the TOA because only an average of ~5.6% of surface thermal emission escapes into space, with the rest absorbed by the atmosphere. Therefore, the inclusion of suppressed surface longwave radiation rather than its TOA value as a positive RF into the calculation of carbon emission equivalents (e.g., Rotenberg and Yakir 2010) may be inappropriate in some cases and can exaggerate the warming effect of the forests on global mean temperature (sometimes by about an order of magnitude in our results).

Longwave RF attributable to altered ET is another important forcing that should be evaluated when inferring the climatic consequences of land-use change. Unlike altered surface albedo or LST, the radiative effect of altered ET is not confined locally to the altered landscape. This nonlocal radiative effect also contrasts

with evaporative cooling, which is pronounced locally. Accurate estimates of such longwave RFs require realistic depictions of the distribution and fate of water vapor, which can be better inferred using integrated climate models than satellite observations (Claussen et al. 2001). For example, climate simulations of global deforestation suggested that the altered ET led to a longwave RF with a magnitude of ~31% of the albedo-induced shortwave RF (Davin et al. 2007). Swann et al. (2010) also found that when planting deciduous trees in the Arctic, the enhanced ET generated a longwave RF up to 1.5 times larger than the shortwave RF from the lowered albedo. Along with these prior findings, our results add further evidence that ET-induced longwave RF at the TOA, unlike that due to altered LST, is not always negligible compared to albedo-induced shortwave RF. Because ET has often been considered as a cooling trend in many studies quantifying the climate value of forests, its warming effect due to the positive longwave RF is often overlooked, potentially overestimating the regional or global cooling of forests.

Uncertainties in estimating RF, net carbon drawdown, and ecosystem greenhouse values can be large, contributing to conflicts in assessing the climate impacts of land-use change. Estimates of carbon sequestration potential sometimes differ for the same forests (e.g., 6 vs. 17 kg/m^2 in Betts [2000] and Montenegro et al. [2009], respectively, for Canadian forests); their potential uncertainty is far larger than our estimated carbon emission equivalent to albedo-induced RF (e.g., 0–5 kg/m^2). Further, conversions from albedo-induced RF to carbon emission equivalent or from carbon sequestration to equivalent RF depend on the time frame over which the impacts of land-use change are examined (Anderson-Teixeira and DeLucia 2011). For example, precise estimates of CO_2-induced RF require characterizing the dynamics of carbon storage after vegetation replacement (O'Halloran et al. 2011). Also, the use of observational data to untangle biophysical processes underlying altered ET remains challenging. Our MODIS-based estimation of ET-induced RF has not captured the full spectrum of interactions and feedbacks associated with altered distributions of water vapor, especially those related to changes in cloud patterns.

Our analyses suggest that the combined effect of albedo reduction and CO_2 uptake on global temperatures was, on average, a cooling for reforestation and afforestation in North America, a finding consistent with that of Montenegro et al. (2009). However, two caveats accompany this estimated cooling effect. First, the local temperature effect of land-use change is determined almost exclusively by biophysical effects, not carbon uptake, regardless of the combined global effect of the two. Second, this global cooling refers only to the net effect of albedo reduction and carbon uptake; therefore, the actual overall effect on global temperature after considering all the biophysical effects will likely be different. Our analysis emphasizes that albedo reduction from planting forests is not the only biophysical forcing affecting temperature (Pielke et al. 2002). Concurrent surface changes in ecophysiological and aerodynamic characteristics alter energy balance and partitioning, sometimes counteracting the local or regional warming of reduced albedo, because of the rougher surface, higher canopy conductance, and deeper roots of forests compared to the replaced vegetation (Jackson et al. 2008, Anderson et al. 2011). The combined effects of these radiative and non-radiative forcings are also moderated by other environmental variables (Juang et al. 2007, Lee et al. 2011). Therefore, whether a given type of land conversion cools or warms the climate depends on its location and extent, as well as the relevant spatial and temporal scales examined (Bonan 2008, Kueppers et al. 2008, Arora and Montenegro 2011).

The use of albedo-induced RF or its carbon emission equivalent metric neglects other biophysical forcings, both radiative and non-radiative (Feddema et al. 2005, Davin et al. 2007). The biophysical forcings of land-use change, including altered sensible and latent heat fluxes, strongly modify the vertical distribution of atmospheric heating, especially at local or regional scales. The redistribution of net surface radiation associated with non-radiative forcings modifies the radiative forcing effect of altered albedo, thus reducing the importance of albedo-induced RF alone on the local/regional temperature response. In fact, Lee et al. (2011) suggested that the main contributor to the warmer air over forests compared to adjacent, more open lands in North America is not their darker surface, because the higher air temperatures over forests were observed most at night when the albedo effect was absent.

The lower daytime surface temperatures that we observed for forests compared to non-forest lands are consistent with other studies that examined effects of vegetation on micrometeorological conditions (Holbo and Luvall 1989, Chen et al. 1993, Jackson et al. 2008, Nosetto et al. 2011). At a site in the southeastern USA at ~36° N, for instance, the grassland had a LST 1.2 K and 0.9 K warmer than did the nearby pine and hardwood forests, respectively (Juang et al. 2007). A U.S. northwestern deciduous forest around 45° N was 4.5 K cooler on a summer day and 2 K warmer at night than a nearby clear-cut (Chen et al. 1993). On the other hand, our data for LST appear to differ from some studies suggesting a local cooling effect of deforestation (i.e., a warming effect of forests). Deforestation in the U.S. Midwest was found to lower both daily maximum and minimum air temperatures with a reduced DTR (Bonan 2001). Direct comparisons are difficult between our study that emphasized changes in LST and those deforestation studies that emphasized near-surface air temperatures, as discussed next.

Assessments of the climate impacts of reforestation and deforestation are confounded by the use of differing temperature metrics (Pielke et al. 2007, Mildrexler et al.

2011). Some studies inferred a cooling effect of forests on air temperature by extrapolating LST data (Juang et al. 2007, Mildrexler et al. 2011). However, Andre et al. (1989) provided a case wherein the LST of a forest relative to adjacent croplands was 2 K cooler, but the air above the forest was 1 K warmer. Rigorous climate assessments of land conversions should explicitly differentiate LST from near-surface air temperatures (i.e., air temperature at 2 m above the displacement height; see Table 1). The two are more likely decoupled at higher values and over smoother surfaces and have been observed to differ by as much as 20 K (Mildrexler et al. 2011). Another complexity is the disparity in physical definitions between three types of temperature for climate research: radiometric, thermodynamic, and aerodynamic temperatures; these metrics are commonly used in remote sensing of surface skin temperature, field measurements of near-surface air temperature, and energy flux calculations in models, respectively (Monteith and Unsworth 2008). Inherent differences between these definitions can sometimes be much larger than the expected climate change signals. For example, radiometric skin temperature can be higher at midday and lower at night than aerodynamic temperature by 2–6 K (Jin and Dickinson 2010). Care is therefore needed to infer climate change signals from temperature data acquired using different protocols.

Evaluating the temperature benefits of forestry activities is also sensitive to the choice of metrics. In terms of RF or carbon metrics, our results suggest that the combined effect of reduced albedo and carbon uptake for most reforestation and afforestation in North America between 20°–60° N is a net global cooling. However, the signs of these RFs or carbon emission equivalent metrics are not always consistent with the actual temperature changes at local and regional scales or even globally (Davin et al. 2007). We further used the change in sensible heat flux as a proxy to quantify the local influence of land conversion on near-surface air temperature, with a positive change indicating a warming effect; this correspondence has been revealed in many observational and modeling studies (Juang et al. 2007, Rotenberg and Yakir 2010, Swann et al. 2010). According to this criterion for our analyses, planting forests with deciduous trees in North America is more likely to locally cool the near-surface air, while planting evergreen forests can cause a local warming in many places (Jackson et al. 2008). Though inferred by comparing the surface biophysics between adjacent sites, this cooling effect of deciduous trees should be interpreted not as lower air temperature compared to adjacent open lands, but instead as the decreased air temperature at a fixed location if the location were forested. Other new metrics have been gradually introduced for climatic assessments that incorporate additional factors (Kueppers et al. 2004, West et al. 2011, Anderson-Teixeira et al. 2012). The availability of multiple metrics is more likely to offer a comprehensive picture, but this may confound practical decision-making if their respective limitations are not made explicit.

The responses of regional and global temperatures to small-scale reforestation and afforestation do not necessarily align with the local response because the dominant mechanisms determining the temperature change can vary across scales (Anderson et al. 2011). This scale-dependence also explains why different metrics (RF of various types or changes in sensible heat) were referred to in this study for assessing the temperature effects of forestry activities and the climatic benefits of ecosystems. Local cooling of forests due to reduced sensible heat fluxes typically comes at a cost of evaporating more water; thus, the degree of such cooling is regulated by constraints such as leaf area, rooting depth, and soil water availability (Jackson et al. 2000, Nosetto et al. 2011). From an aerodynamic perspective, there is often a strong mixing between air and forested surfaces or, alternatively speaking, a closer coupling of LST to air temperature. Therefore, when the near-surface air is cooler than the surface, especially at midday, forest canopy structures promote turbulence to cool the surface (Nemani et al. 1993, Mildrexler et al. 2011), likely with a magnitude outweighing the warming effect of lowered albedo of forests; at night, when the albedo-induced warming effect varnishes and the air is likely warmer than the surface, the turbulent mixing over the forest slows down the surface cooling compared to nearly open lands (Nemani et al. 1993, Lee et al. 2011). Beyond local scales, the mechanisms involve many feedbacks. For example, enhanced ET not only contributes to the greenhouse warming effect of water vapor, but also leads to some negative feedbacks related to lapse rate and cloud formation. Although some ideal experiments showed that the increased ET at the global level cooled the climate due to water vapor–clouds feedback (Ban-Weiss et al. 2011), its effects in more realistic land-cover change scenarios remain uncertain.

By demonstrating the importance of biophysical forcings of land-use change, our work helps to resolve previous discrepancies regarding the climatic benefits of forests and also challenges some existing ways of addressing biophysics in evaluating net climate benefits (Rotenberg and Yakir 2010, Anderson et al. 2011). We emphasize that the accounting of albedo along with carbon is better than using carbon alone, but in many cases is still inadequate for inferring the temperature effect of forestry projects. Our results suggest that neglecting other important radiative and non-radiative forcings will overestimate the global cooling benefit of planting trees in many locations. This overestimation partially explains why the use of RF-related metrics suggested a cooling from reforestation at high latitudes, yet some modeling studies indicated the opposite (Bala et al. 2007, Montenegro et al. 2009).

Incorporating biophysical impacts of forestry activities into climate policies is needed but remains challeng-

ing (Anderson et al. 2011). The failure to consider biophysical effects may exaggerate the climate benefits of forestry projects for climate regulation, thus reducing the actual value of such projects. However, no consensus has yet been reached on how to value biophysical forcings of forests in relation to carbon sequestration, especially given their possibly differing climate responses if examined at different spatial or temporal scales (Bonan 2008). Our current understanding of the biophysical influences of forests on climate is also evolving. In addition to surface biophysics, many forcings and interactions for local land-use changes, such as changed lapse rate and cloud feedbacks, should be further elucidated for quantifying the full range of biophysical forcings (National Research Council 2005). This complexity in ecosystem–air interactions argues for flexible and robust policy designs that, ideally, incorporate new understanding of land-use impacts as the science advances. Successful climate policies should also acknowledge a trade-off at times with other nonclimatic consequences, such as water availability, soil fertility, and the economics of land use (Jackson et al. 2005). Integrating multiple policies thus becomes important for promoting ecological, environmental, and social-economic sustainability of land-use and forestry activities.

Summary

Biological carbon sequestration by reforestation and afforestation is being promoted as an opportunity to help mitigate global warming and climate change. The scientific basis to support such forestry activities is shifting to include many biophysical dimensions beyond carbon storage. Darker trees absorb more sunlight and counteract some of the cooling from carbon uptake. The net effect of reduced albedo and CO_2 from forestry activities is typically assessed by converting albedo-induced RF to carbon emission equivalents for comparison against the amount of CO_2 drawdown by the forest. The utility of the resultant metric for evaluating global mean near-surface temperature is questionable, due at least to its inability to account for (1) the difference in climate sensitivity between albedo-induced shortwave and CO_2-induced longwave RFs, (2) other non-radiative or radiative biophysical forcings, and (3) the spatial and temporal variations in temperature responses. At local or regional scales, the warming effect of reduced albedo is strongly moderated by other biophysical forcings associated with generally higher surface roughness and canopy conductance of forests, via either direct modifications of surface energy fluxes or indirect interactions and feedbacks. Enhanced ET from trees yields a direct cooling effect on LST and also tends to indirectly cool near-surface air by reducing the input of sensible heat to the air. The sign of change in sensible heat flux can indicate the net local effect of reforestation and afforestation on air temperature.

In our analyses for North America, the spatial pattern in temperature responses to potential reforestation/afforestation showed strong geographic variations, but cannot be explained solely by latitude. Our analyses suggest that forestry activities will have the most climatic benefits at locations where background albedo prior to landscape change is low, snow cover is minimal, cloud cover is high, and soil water availability is ample. Our results also suggest that forestry projects with deciduous trees are likely to produce larger biophysical benefits than those with evergreen trees.

Acknowledgments

This work was supported by DOE's National Institute for Climatic Change Research, the U.S. Department of Agriculture (number 2012-68002-19795), and the National Center for Ecological Analysis and Synthesis. We thank Gordon Bonan, Noah Diffenbaugh, Qiaozhen Mu, members of the Jackson Lab, and three anonymous reviewers for useful suggestions on the manuscript. Special thanks go to Lara Kueppers and Yaqiong Lu for their assistance and discussion of the WRF-CLM model.

Literature Cited

Anderson, R. G., et al. 2011. Biophysical considerations in forestry for climate protection. Frontiers in Ecology and the Environment 9:174–182.

Anderson-Teixeira, K. J., and E. H. DeLucia. 2011. The greenhouse gas value of ecosystems. Global Change Biology 17:425–438.

Anderson-Teixeira, K. J., P. K. Snyder, T. E. Twine, S. V. Cuadra, M. H. Costa, and E. H. DeLucia. 2012. Climate-regulation services of natural and agricultural ecoregions of the Americas. Nature Climate Change 2:177–181.

Andre, J. C., P. Bougeault, J. F. Mahfouf, P. Mascart, J. Noilhan, and J. P. Pinty. 1989. Impact of forests on mesoscale meteorology. Philosophical Transactions of the Royal Society of London Series B 324:407–422.

Andrews, T., P. M. Forster, and J. M. Gregory. 2009. A surface energy perspective on climate change. Journal of Climate 22:2557–2570.

Arora, V. K., and A. Montenegro. 2011. Small temperature benefits provided by realistic afforestation efforts. Nature Geoscience 4:514–518.

Bala, G., K. Caldeira, M. Wickett, T. J. Phillips, D. B. Lobell, C. Delire, and A. Mirin. 2007. Combined climate and carbon-cycle effects of large-scale deforestation. Proceedings of the National Academy of Sciences USA 104:6550–6555.

Ban-Weiss, G. A., G. Bala, L. Cao, J. Pongratz, and K. Caldeira. 2011. Climate forcing and response to idealized changes in surface latent and sensible heat. Environmental Research Letters 6:034032.

Betts, R. A. 2000. Offset of the potential carbon sink from boreal forestation by decreases in surface albedo. Nature 408:187–190.

Bonan, G. B. 2001. Observational evidence for reduction of daily maximum temperature by croplands in the Midwest United States. Journal of Climate 14:2430–2442.

Bonan, G. B. 2002. Ecological climatology: concepts and applications. Cambridge University Press, Cambridge, UK.

Bonan, G. B. 2008. Forests and climate change: Forcings, feedbacks, and the climate benefits of forests. Science 320:1444–1449.

Brovkin, V., M. Claussen, E. Driesschaert, T. Fichefet, D. Kicklighter, M. F. Loutre, H. D. Matthews, N. Ramankutty, M. Schaeffer, and A. Sokolov. 2006. Biogeophysical effects of historical land cover changes simulated by six Earth system models of intermediate complexity. Climate Dynamics 26:587–600.

Chen, J. Q., J. F. Franklin, and T. A. Spies. 1993. An empirical-model for predicting diurnal air-temperature gradients from edge into old-growth Douglas-fir forest. Ecological Modelling 67:179–198.

Claussen, M., V. Brovkin, and A. Ganopolski. 2001. Biogeophysical versus biogeochemical feedbacks of large-scale land cover change. Geophysical Research Letters 28:1011–1014.

Collins, W. D., et al. 2006. Radiative forcing by well-mixed greenhouse gases: Estimates from climate models in the Intergovernmental Panel on Climate Change (IPCC) Fourth Assessment Report (AR4). Journal of Geophysical Research—Atmospheres 111:D14317.

Costa, S. M. S., and K. P. Shine. 2012. Outgoing longwave radiation due to directly transmitted surface emission. Journal of the Atmospheric Sciences 69:1865–1870.

Davin, E. L., N. de Noblet-Ducoudre, and P. Friedlingstein. 2007. Impact of land cover change on surface climate: Relevance of the radiative forcing concept. Geophysical Research Letters 34:L13702.

Diffenbaugh, N. S. 2009. Influence of modern land cover on the climate of the United States. Climate Dynamics 33:945–958.

Donohoe, A., and D. S. Battisti. 2011. Atmospheric and surface contributions to planetary albedo. Journal of Climate 24:4402–4418.

Feddema, J. J., K. W. Oleson, G. B. Bonan, L. O. Mearns, L. E. Buja, G. A. Meehl, and W. M. Washington. 2005. The importance of land-cover change in simulating future climates. Science 310:1674–1678.

Friedl, M. A., et al. 2002. Global land cover mapping from MODIS: algorithms and early results. Remote Sensing of Environment 83:287–302.

Gibbard, S., K. Caldeira, G. Bala, T. J. Phillips, and M. Wickett. 2005. Climate effects of global land cover change. Geophysical Research Letters 32:L23705.

Hansen, J., et al. 2005. Efficacy of climate forcings. Journal of Geophysical Research—Atmospheres 110:D18104.

Heimann, M., and M. Reichstein. 2008. Terrestrial ecosystem carbon dynamics and climate feedbacks. Nature 451:289–292.

Holbo, H. R., and J. C. Luvall. 1989. Modeling surface-temperature distributions in forest landscapes. Remote Sensing of Environment 27:11–24.

Houghton, R. A. 2003. Revised estimates of the annual net flux of carbon to the atmosphere from changes in land use and land management 1850–2000. Tellus Series B Chemical and Physical Meteorology 55:378–390.

Jackson, R. B., and J. S. Baker. 2010. Opportunities and constraints for forest climate mitigation. Bioscience 60:698–707.

Jackson, R. B., E. G. Jobbagy, R. Avissar, S. B. Roy, D. J. Barrett, C. W. Cook, K. A. Farley, D. C. le Maitre, B. A. McCarl, and B. C. Murray. 2005. Trading water for carbon with biological sequestration. Science 310:1944–1947.

Jackson, R. B., et al. 2008. Protecting climate with forests. Environmental Research Letters 3:044006.

Jackson, R. B., et al. 2000. Belowground consequences of vegetation change and their treatment in models. Ecological Applications 10:470–483.

Jayawickreme, D. H., C. S. Santoni, J. H. Kim, E. G. Jobbagy, and R. B. Jackson. 2011. Changes in hydrology and salinity accompanying a century of agricultural conversion in Argentina. Ecological Applications 21:2367–2379.

Jin, M. L., and R. E. Dickinson. 2010. Land surface skin temperature climatology: benefitting from the strengths of satellite observations. Environmental Research Letters 5:044004.

Juang, J.-Y., G. Katul, M. Siqueira, P. Stoy, and K. Novick. 2007. Separating the effects of albedo from eco-physiological changes on surface temperature along a successional chronosequence in the southeastern United States. Geophysical Research Letters 34:L21408.

Kelly, R. E., A. T. Chang, L. Tsang, and J. L. Foster. 2003. A prototype AMSR-E global snow area and snow depth algorithm. IEEE Transactions on Geoscience and Remote Sensing 41:230–242.

Kueppers, L. M., P. Baer, J. Harte, B. Haya, L. E. Koteen, and M. E. Smith. 2004. A decision matrix approach to evaluating the impacts of land-use activities undertaken to mitigate climate change - An editorial essay. Climatic Change 63:247–257.

Kueppers, L. M., M. A. Snyder, and L. C. Sloan. 2007. Irrigation cooling effect: Regional climate forcing by land-use change. Geophysical Research Letters 34:L03703.

Kueppers, L. M., et al. 2008. Seasonal temperature responses to land-use change in the western United States. Global and Planetary Change 60:250–264.

Lee, X., M. L. Goulden, D. Y. Hollinger, A. Barr, T. A. Black, G. Bohrer, R. Bracho, B. Drake, A. Goldstein, and L. Gu. 2011. Observed increase in local cooling effect of deforestation at higher latitudes. Nature 479:384–387.

Liou, K. N. 2002. An introduction to atmospheric radiation. Second edition. Academic Press, Amsterdam, The Netherlands.

Lu, Y., and L. M. Kueppers. 2012. Surface energy partitioning over four dominant vegetation types across the United States in a coupled regional climate model (Weather Research and Forecasting Model 3-Community Land Model 3.5). Journal of Geophysical Research 117:D06111.

Matthews, H. D., A. J. Weaver, M. Eby, and K. J. Meissner. 2003. Radiative forcing of climate by historical land cover change. Geophysical Research Letters 30:1055.

McAlpine, C. A., J. G. Ryan, L. Seabrook, S. Thomas, P. J. Dargusch, J. I. Syktus, R. A. Pielke, A. E. Etter, P. M. Fearnside, and W. F. Laurance. 2010. More than CO(2): a broader paradigm for managing climate change and variability to avoid ecosystem collapse. Current Opinion in Environmental Sustainability 2:334–346.

McKinley, D. C., et al. 2011. A synthesis of current knowledge on forests and carbon storage in the United States. Ecological Applications 21:1902–1924.

Mildrexler, D. J., M. Zhao, S. W. Running, G. Hugelius, T. Virtanen, D. Kaverin, A. Pastukhov, F. Rivkin, S. Marchenko, and V. Romanovsky. 2011. A global comparison between station air temperatures and MODIS land surface temperatures reveals the cooling role of forests. Journal of Geophysical Research 116:G03025.

Monteith, J. L., and M. H. Unsworth. 2008. Principles of environmental physics. Elsevier Academic Press, New York, New York, USA.

Montenegro, A., M. Eby, Q. Z. Mu, M. Mulligan, A. J. Weaver, E. C. Wiebe, and M. S. Zhao. 2009. The net carbon drawdown of small scale afforestation from satellite observations. Global and Planetary Change 69:195–204.

Mu, Q., M. Zhao, and S. W. Running. 2011. Improvements to a MODIS global terrestrial evapotranspiration algorithm. Remote Sensing of Environment 115:1781–1800.

National Research Council. 2005. Radiative forcing of climate change: Expanding the concept and addressing uncertainties. National Academies Press, Washington, D.C., USA.

Nemani, R., L. Pierce, S. Running, and S. Goward. 1993. Developing satellite-derived estimates of surface moisture status. Journal of Applied Meteorology 32:548–557.

Nosetto, M. D., E. G. Jobággy, A. B. Brizuela, and R. B. Jackson. 2011. The hydrologic consequences of land cover change in central Argentina. Agriculture, Ecosystems and Environment 154:2–11.

O'Halloran, T. L., B. E. Law, M. L. Goulden, Z. Wang, J. G. Barr, C. Schaaf, M. Brown, J. D. Fuentes, M. Göckede, and A. Black. 2011. Radiative forcing of natural forest disturbances. Global Change Biology 18:555–565.

Pervez, M. S., and J. F. Brown. 2010. Mapping irrigated lands at 250-m scale by merging MODIS data and national agricultural statistics. Remote Sensing 2:2388–2412.
Pielke, R. A., et al. 2007. Unresolved issues with the assessment of multidecadal global land surface temperature trends. Journal of Geophysical Research—Atmospheres 112:D24S08.
Pielke, R. A., G. Marland, R. A. Betts, T. N. Chase, J. L. Eastman, J. O. Niles, D. S. Niyogi, and S. W. Running. 2002. The influence of land-use change and landscape dynamics on the climate system: relevance to climate-change policy beyond the radiative effect of greenhouse gases. Philosophical Transactions of the Royal Society of London A 360:1705–1719.
Pongratz, J., T. Raddatz, C. H. Reick, M. Esch, and M. Claussen. 2009. Radiative forcing from anthropogenic land cover change since A.D. 800. Geophysical Research Letters 36:L02709.
Randerson, J. T., et al. 2006. The impact of boreal forest fire on climate warming. Science 314:1130–1132.
Rotenberg, E., and D. Yakir. 2010. Contribution of semi-arid forests to the climate system. Science 327:451–454.
Schaaf, C. B., et al. 2002. First operational BRDF, albedo nadir reflectance products from MODIS. Remote Sensing of Environment 83:135–148.
Swann, A. L., I. Y. Fung, S. Levis, G. B. Bonan, and S. C. Doney. 2010. Changes in Arctic vegetation amplify high-latitude warming through the greenhouse effect. Proceedings of the National Academy of Sciences USA 107:1295–1300.
Trenberth, K. E., J. T. Fasullo, and J. Kiehl. 2009. Earth's global energy budget. Bulletin of the American Meteorological Society 90:311–323.
Wan, Z., Y. Zhang, Q. Zhang, and Z.-L. Li. 2004. Quality assessment and validation of the MODIS global land surface temperature. International Journal of Remote Sensing 25:261–274.
West, P. C., G. T. Narisma, C. C. Barford, C. J. Kucharik, and J. A. Foley. 2011. An alternative approach for quantifying climate regulation by ecosystems. Frontiers in Ecology and the Environment 9:126–133.
Wielicki, B. A., et al. 1998. Clouds and the Earth's Radiant Energy System (CERES): Algorithm overview. IEEE Transactions on Geoscience and Remote Sensing 36:1127–1141.

Supplemental Material

Appendix

Complementary results from remote-sensing data analyses: maps of vegetation distributions; latitudinal and seasonal patterns of surface albedo, land surface temperature, and evapotranspiration for the four vegetation types considered; snowfall patterns; and spatial patterns of cloud fraction and atmospheric optical properties (*Ecological Archives* M084-011-A1).

Data Availability

Data associated with this paper have been deposited in the Oak Ridge National Laboratory Distributed Active Archive Center for Biogeochemical Dynamics: http://dx.doi.org/10.3334/ORNLDAAC/1210